Available online at www.sciencedirect.com

ScienceDirect

Geochimica et Cosmochimica Acta 163 (2015) 279–298

Geochimica et Cosmochimica Acta

www.elsevier.com/locate/gca

Os–Nd–Sr isotopes in Miocene ultrapotassic rocks of southern Tibet: Partial melting of a pyroxenite-bearing lithospheric mantle?

Feng Huang [a,b], Jian-Lin Chen [a,c], Ji-Feng Xu [a,c,*], Bao-Di Wang [d], Jie Li [a]

[a] State Key Laboratory of Isotope Geochemistry, Guangzhou Institute of Geochemistry, Chinese Academy of Sciences, Guangzhou 510640, PR China

[b] University of Chinese Academy of Sciences, Beijing 100049, PR China

[c] CAS Center for Excellence in Tibetan Plateau Earth Sciences, PR China

[d] Chengdu Institute of Geology and Mineral Resources, Chengdu 610081, PR China

Received 14 August 2014; accepted in revised form 30 April 2015; Available online 7 May 2015

Abstract

Miocene post-collisional ultrapotassic rocks in the southern and central parts of the Lhasa Terrane of southern Tibet provide an opportunity to explore the deep processes and lithospheric evolution of the Tibetan Plateau. The magmatic source of the ultrapotassic rocks is still debated. However, the source can be identified using the Re–Os isotopic system. In this paper, we provide comprehensive data on the Re–Os isotopic compositions of ultrapotassic rocks from Mibale and Maiga areas in southern Tibet, and we refine the age of the Mibale ultrapotassic rocks to 12.5 Ma. The Os isotopic data demonstrate that crustal assimilation affected the Os isotopic compositions of some ultrapotassic rocks with low Os contents, but samples with high Os contents have little or no evidence of crustal contamination. The initial $^{187}Os/^{188}Os$ ratios of the least-contaminated ultrapotassic rocks are higher than those of primitive upper mantle (PUM). The ultrapotassic rocks show a weak correlation between initial $^{187}Os/^{188}Os$ ratios and Mg# values, a negative correlation between $\varepsilon_{Nd}(t)$ and Mg# values, and high Ni contents and FeO/MnO ratios. These observations indicate that the ultrapotassic rocks were derived from a pyroxenite-bearing lithospheric mantle. Simple calculations indicate <20% pyroxenite in the lithospheric mantle, which is consistent with the pyroxenite xenoliths found in the ultrapotassic rocks of southern Tibet. The Os model ages for the ultrapotassic rocks in the south Lhasa Terrane range from 75 to 541 Ma, indicating that the lithospheric mantle beneath southern Tibet underwent multiple magmatic events. We conclude, therefore, that convective removal of a pyroxenite-bearing lithospheric mantle or break-off of the Indian continental lithospheric mantle could have resulted in the generation of the ultrapotassic rocks in southern Tibet.

1. INTRODUCTION

It is generally accepted that the expansive Tibetan Plateau and surrounding mountain ranges are direct consequences of the collision of the Indian and Asian continents in the late Mesozoic–early Cenozoic (Rowley, 1996; Yin and Harrison, 2000; Mo et al., 2007). Ultrapotassic and potassic rocks were widely distributed in the southern and

* Corresponding author at: State Key Laboratory of Isotope Geochemistry, Guangzhou Institute of Geochemistry, Chinese Academy of Sciences, Guangzhou 510640, PR China. Tel.: +86 20 85290282; fax: +86 20 85290130.

E-mail address: jifengxu@gig.ac.cn (J.-F. Xu).

http://dx.doi.org/10.1016/j.gca.2015.04.053

0016-7037/

central parts of the Lhasa Terrane of southern Tibet after the collision (Turner et al., 1996; Miller et al., 1999; Ding et al., 2003; Williams et al., 2004; Chung et al., 2005; Zhao et al., 2006, 2009; Gao et al., 2007a,b; Guo et al., 2013; Liu et al., 2014b), and this post-collisional ultrapotassic magmatism offers a unique opportunity to constrain the deep mantle and dynamic processes that created the highest plateau in the world. Although many researchers have investigated these ultrapotassic lavas, their petrogenesis remains controversial (Turner et al., 1996; Miller et al., 1999; Ding et al., 2003; Williams et al., 2004; Chung et al., 2005; Guo et al., 2006, 2013; Gao et al., 2007b, 2009, 2010; Zhao et al., 2009; Chen et al., 2010, 2012a,b; Liu et al., 2013, 2014b). There are three main hypotheses for explaining the post-collisional ultrapotassic rocks: (1) convective removal of a previously metasomatized lithospheric mantle (Turner et al., 1996; Miller et al., 1999; Williams et al., 2004; Liu et al., 2011), (2) intracontinental subduction of the Indian continental lithosphere (Ding et al., 2003; Gao et al., 2007b; Zhao et al., 2009), and (3) break-off of a northwards subducted slab of the Indian continental lithosphere (Kohn and Parkinson, 2002; Maheo et al., 2002). Most recently it has been proposed that mixing of the asthenospheric mantle wedge with fluids and/or melts derived from subducted crust led to the genesis of the ultrapotassic volcanic rocks (Guo et al., 2013), and that the crust of the ancient Lhasa Terrane may have contributed to the ultrapotassic magmas (Liu et al., 2013, 2014b).

To understand the petrogenesis of ultrapotassic magmas in relation to the evolution of geodynamic condition at deep levels, we concentrated our study on the Mibale and Maiga ultrapotassic volcanic rocks of southern Tibet (Fig. 1a), which are typical ultrapotassic rocks with high MgO contents (Ding et al., 2006; Gao et al., 2007b; Zhao et al., 2009; Guo et al., 2013). Although data on the major and trace elements, and Sr–Nd isotopes of these volcanics have been published, the traditional data for radiogenic Sr–Nd isotopes are not ideal for providing sufficient information on magma sources because of possible contamination by crust or sediment-derived melts/fluids; this problem arises because of the similar behavior of

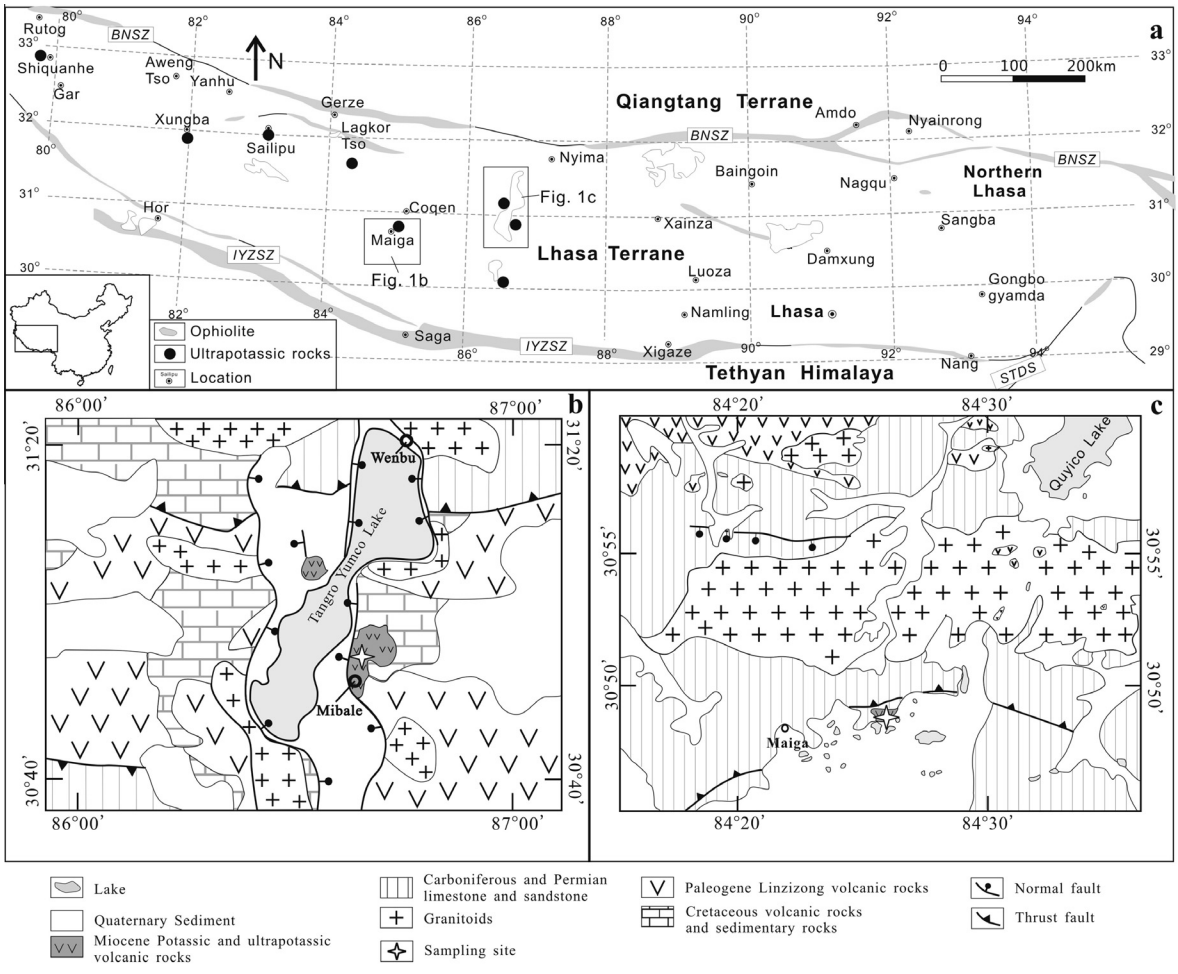

Fig. 1. (a) Map of southern Tibet showing the major terranes and the temporal and spatial distribution of Miocene ultrapotassic rocks (modified from Chung et al., 2005 and Zhao et al., 2009). (b) Simplified geological map showing outcrops of ultrapotassic rocks in Mibale (modified from Ding et al., 2003 and Guo et al., 2013). (c) Simplified geological map showing outcrops of ultrapotassic rocks in Maiga (modified from Chen, 2007).

radioactive mother-daughter isotopes during both partial melting and fluid activity. The Re–Os isotope system provides a way of overcoming this problem because Re is a moderately incompatible element whereas Os is a compatible element during partial melting of mantle peridotite, thereby making it possible to distinguish the Os isotopic characteristics of crust, lithospheric mantle, and asthenospheric mantle (Shirey and Walker, 1998; Xu et al., 2007; Callegaro et al., 2013). In this paper we provide high-precision Re–Os isotope data, and in combination with previous research, our comprehensive Os–Nd–Sr isotopic investigations of the ultrapotassic rocks of southern Tibet allow us to evaluate the source of the ultrapotassic volcanic rocks as well as constrain the dynamic mechanisms involved in the formation of the Tibetan Plateau.

2. GEOLOGICAL SETTING

The Tibetan Plateau, which is composed of many blocks that were involved in collisional and accretionary processes throughout the Paleozoic and Cenozoic, consists of the Songpan-Ganzi, Qiangtang, and Lhasa terranes, from north to south (Fig. 1a; Yin and Harrison, 2000; Royden et al., 2008; Pan et al., 2012; Zhu et al., 2013). The Lhasa Terrane is located in southern Tibet, and is bounded by the Bangong-Nujiang suture (BNS) to the north and the Indus-Yarlung-Zangbo suture (IYZS) to the south (Yin and Harrison, 2000). It is generally accepted that the IYZS marks the closure of the Neo-Tethys Ocean and the subsequent collision of India and Asia at ca. 65 Ma (Yin and Harrison, 2000; Mo et al., 2007). The southern part of the Lhasa Terrane is typified by the Andean-type calc-alkaline Linzizong volcanics and the Gangdese batholith (Early Jurassic to Eocene, Zhou et al., 2004; Mo et al., 2007, 2008; Ji et al., 2009; Lee et al., 2009, 2012; Zhu et al., 2011; Zhang et al., 2013). All this magmatism was caused by the northwards subduction of the Neo-Tethyan lithosphere and the subsequent India-Eurasia collision.

Volumetrically minor, post-collisional potassic-ultrapotassic lavas and dikes, adakitic dikes and intrusions are widely distributed in southern Tibet, and they represent the intraplate magmatism that took place after the cessation of subduction-related volcanism (Owens and Zandt, 1997; Chung et al., 2005). The ultrapotassic rocks in this region are defined as having $K_2O/Na_2O > 2$, $K_2O > 3$ wt%, and MgO > 3 wt%, based on whole-rock chemistry (Foley et al., 1987), and they generally occur west of 87°E (Zhao et al., 2006, 2009). This paper mainly focuses on the relatively high-MgO ultrapotassic rocks in southern Tibet, as they are perhaps the closest in their compositions to the original magmas.

The ultrapotassic rocks studied in this paper were collected from the Maiga and Mibale areas (Fig. 1a). The Mibale ultrapotassic rocks were nearly all erupted in the middle of the N–S trending Tangro Yumco-Xuruco Graben at 12.6–19 Ma (Table 1, Fig. 1a; Liao et al., 2002; Xie et al., 2004; Gao et al., 2007b; Zhou et al., 2009; Guo et al., 2013), and they overlie Cretaceous sedimentary rocks and the Linzizong volcanics. The Tangro Yumco-Xuruco Graben is located in the mid-western part of the Lhasa Terrane. It is the largest graben in southern Tibet (Blisniuk et al., 2001; Kapp et al., 2007; Royden et al., 2008), and it contains numerous examples of small-volume Miocene ultrapotassic volcanic rocks (Fig. 1b).

The Maiga ultrapotassic rocks are located in the mid-northern region of the Gangdese batholith, about 150 km west of Mibale (Fig. 1a), and they form small lava mounds that were erupted at ca. 17 Ma (Table 1; Ding et al., 2006; Chen, 2007). These ultrapotassic rocks directly overlie Carboniferous and Permian sedimentary rocks (Fig. 1c).

The ultrapotassic rocks in both areas typically display porphyritic textures, with abundant phenocrysts up to 2–4 mm in diameter set in a fine groundmass. The main phenocryst phases are olivine, diopside, K-feldspar, phlogopite, and biotite, with lesser amounts of amphibole, coupled with minor accessory minerals such as Fe-Ti oxides, apatite, and zircon. The groundmass has a trachytic texture and consists of microcrystalline laths of K-feldspar, biotite, glass, and minor opaque minerals. More details and further sample descriptions can be found in previous papers (Zhao et al., 2006, 2009; Gao et al., 2007b; Guo et al., 2013).

3. ANALYTICAL METHODS

Zircon, as an accessory mineral in various types of magmatic rocks, can effectively preserve the U–Pb isotopic ratios of the igneous material. We chose sample CM10-04-03 from Mibale, and separated the zircons to determine an accurate eruption age, using U–Pb isotope analyses obtained with the sensitive high-resolution ion microprobe II (SHRIMP II) at the Institution of Geology, Chinese Academy of Geological Sciences,

Table 1
Age of the ultrapotassic rocks in Mibale and Maiga, southern Tibet.

Locality	Sample	Dating method	Mineral or whole rock dated	Age (Ma)	References
Mibale	CM10-04-03	U–Pb	Zircon	12.5 ± 0.5	This study
Mibale	8030-5	K–Ar	Whole rock	19.04 ± 0.97	Xie et al. (2004)
Mibale	8030-5	K–Ar	Whole rock	12.60 ± 0.97	Liao et al. (2002)
Mibale	8030-5	$^{40}Ar/^{39}Ar$	Whole rock	13.47 ± 0.13	Zhou et al. (2009)
Mibale	8030-18	K–Ar	Whole rock	14.22 ± 0.68	Xie et al. (2004)
Mibale	8030-18	$^{40}Ar/^{39}Ar$	Whole rock	13.17 ± 0.11	Zhou et al. (2009)
Maiga	2003T405	$^{40}Ar/^{39}Ar$	Phlogopite	17.4 ± 0.1	Ding et al. (2006)
Maiga	CQQ4-04-02	$^{40}Ar/^{39}Ar$	K-feldspar	16.28 ± 0.07	Chen (2007)

Beijing, China. Zircons were mounted with a fragment of the reference zircon SL 13 (572 Ma, U = 238 ppm) (Williams et al., 1996) and with grains of the standard zircon TEM (417 Ma, with variable U contents) (Black et al., 2003). External standardization was by analysis of NIST SRM 610. Common Pb corrections were based on the measured $^{204}Pb/^{206}Pb$ and/or $^{208}Pb/^{206}Pb$ ratios, as described in Compston et al. (1992). Errors for individual analyses are given at the 1-sigma level (Table A1) and were determined from counting statistics and time-dependent correction of the standard. The chi-squared (χ^2) test was employed to assess if an age population met the statistical requirements. When $\chi^2 = 1$, the error of the weighted mean age is consistent with the error of individual analyses, and there is no excess scatter (Black and Jagodzinski, 2003). For details of the operating conditions of the SHRIMP II and data correction, see Jian et al. (2012).

Selected whole-rock samples (any weathered surfaces were removed, and mostly fresh samples were chosen for analysis) were first split into small blocks and ultrasonically cleaned in distilled water with 5% HNO_3, and then washed with distilled water alone. After drying, fresh samples were handpicked. The rocks were crushed and ground in an agate ring mill, and the final powder was used for analyses of major and trace elements as well as Sr–Nd isotopes. Major elements were determined using X-ray fluorescence (XRF) spectrometry, whereas trace element contents were measured with a PE Elan 6000 inductively coupled-plasma mass spectrometer (ICP-MS) at the Guangzhou Institute of Geochemistry, Chinese Academy of Sciences (GIGCAS), Guangzhou, China. Analytical uncertainties are ±1–3% for major elements. The uncertainties in the analyses of internal standards and trace elements are ±5% for REEs and ±5–10% for trace elements. The analytical procedures followed those described by Chen et al. (2010).

Sr and Nd isotope contents were measured using a Micromass Isoprobe multicollector-inductively coupled plasma-mass spectrometer (MC-ICP-MS), also at GIGCAS. The analytical procedures for measuring Sr and Nd isotope contents are described in detail by Li et al. (2004) and Wei et al. (2002). The methods used for the chemical separation of Sr and Nd were similar to those described by Aikman et al. (2012) and Chen et al. (2010). The $^{87}Sr/^{86}Sr$ value of the NBS 987 standard and the $^{143}Nd/^{144}Nd$ value of the JNdi-1 standard were 0.710282 ± 20 (2σ) and 0.512116 ± 11 (2σ), respectively, and all measured $^{143}Nd/^{144}Nd$ and $^{86}Sr/^{88}Sr$ ratios were fractionation corrected to $^{146}Nd/^{144}Nd = 0.7129$ and $^{86}Sr/^{88}Sr = 0.1194$, respectively.

The samples for Re–Os isotopic analysis were split into small chips using a hammer wrapped in paper to avoid contamination, and the chips were then soaked in 4N HCl for half an hour. After rinsing in distilled water, selected rock chips were crushed by hand in an agate mortar, providing 5–10 g powder. Approximately 2 g of the sample powder (spiked with ^{190}Os and ^{185}Re) was then dissolved in aqua regis, frozen in a Carius tube and sealed, then heated at 240 °C for 24 h for digestion (Shirey and Walker, 1995). After opening the Carius tube, Os was extracted with CCl_4 and back-extracted into HBr (Cohen and Waters, 1996; Pearson and Woodland, 2000). After Os had been separated, the remaining Re-containing solution was dried and re-dissolved in HCl. The Re was then separated and purified in an anion exchange column (AG1X8 resin, 100–200 meshes). Finally, the Re isotopes were measured by isotope dilution-inductively coupled plasma-mass spectrometry (ID-ICP-MS, Thermo-Scientific XSERIES-2). Before the Os contents were measured with a thermal ionization mass spectrometer (N-TIMS, Thermo-Finnigan TRITON), the Os was purified by micro-distillation, and the isotopic abundances of OsO_3^- and ReO_4^- were measured on a Thermo-Finnigan Triton mass spectrometer in negative ion detection mode (Creaser et al., 1991; Volkening et al., 1991). Equipped with an oxygen gas leak valve and an ion counting multiplier, the Os was loaded onto a high-purity Pt filament (99.999%, 1 × 0.025 mm) that had already been heated in air for more than 3 min. The Re and Os isotope compositions were measured using a static multiple Faraday collector and a pulse counting electron multiplier, respectively. The instrumental mass fractionation of Os was corrected by normalizing the measured $^{192}Os/^{188}Os$ ratio to 3.08271. Oxide corrections were made using $^{17}O/^{16}O = 0.00037$ and $^{18}O/^{16}O = 0.002047$ (Nier, 1950). Both Re and Os were corrected for blanks. Total blank levels were 7.1 ± 0.3 (2σ) and 2.0 ± 0.4 (2σ) pg for Re and Os, respectively, and the blank $^{187}Os/^{188}Os$ ratio was 0.298 ± 0.030 (2σ). The contributions of the blanks to the measured Os and Re contents were minor (<1%). The Re–Os isotopic analyses of the Mibale and Maiga ultrapotassic rocks were undertaken at the Japan Agency for Marine-Earth Science and Technology (JAMSTEC), Yokosuka, Japan, and at GIGCAS, respectively. Repeat analyses of the ultrapotassic rocks in the two laboratories show consistent results. The details of the analytical procedures are described by Li et al. (2010, 2014) and Xu et al. (2007).

4. RESULTS

4.1. Age data

The analytical results are listed in Appendix Table A1. The Th/U ratios of zircons range from 0.69 to 6.01, which

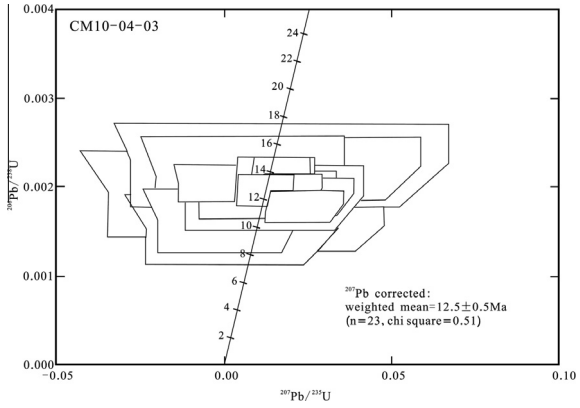

Fig. 2. Zircon U–Pb concordia diagram for sample CM10-04-03 from Mibale, southern Tibet (see the text for details).

suggest they are typical igneous zircons (Hoskin and Schaltegger, 2003) with crystallization ages that could represent the age of the formation of the Mibale ultrapotassic rocks. The ^{207}Pb-corrected weighted mean age is 12.5 ± 0.5 Ma (Fig. 2), close to that given in previous studies (Table 1) with the exception of two inherited zircons that gave inherited ages of 164.4 and 51.6 Ma (Table A1). The common Pb correction procedure follows Compston et al. (1992) and Jian et al. (2012).

4.2. Major and trace elements

The Mibale ultrapotassic volcanic rocks belong to the alkaline series, and they plot mainly as trachyandesite and trachyte on a TAS diagram (Fig. 3). The MgO contents of our samples exceed 3 wt%, except for sample CM10-04-20 (Table A2). The Maiga ultrapotassic rocks exhibit a small range in composition, and they all plot in the trachyandesite field. The major element contents of the Maiga ultrapotassic rocks are similar to those of the Mibale trachyandesites except for the MgO contents which are much higher and exceed 9 wt%.

Chondrite-normalized REE patterns for the Mibale and Maiga ultrapotassic rocks exhibit the same geochemical signatures, including a strong enrichment in light rare earth elements (LREEs) and weak negative Eu anomalies (Mibale, δEu = 0.55–0.96; Maiga, δEu = 0.59–0.76). Primitive-mantle-normalized trace element spider diagrams for the Mibale and Maiga volcanic rocks (Fig. 4) exhibit enrichment in large ion lithophile elements (LILEs; e.g., Rb, Ba) and depletion in high field strong elements (HFSEs) such as Nb, Ta, and Ti. Ba and Sr show obvious negative anomalies, though they have high concentrations.

4.3. Sr–Nd isotopes

Initial Sr–Nd isotopic ratios were calculated using the average ages of the two volcanic fields (Table 2). The initial ^{87}Sr/^{86}Sr ratios of the Mibale and Maiga ultrapotassic rocks are in the ranges 0.7191–0.7207 and 0.7219–0.7220,

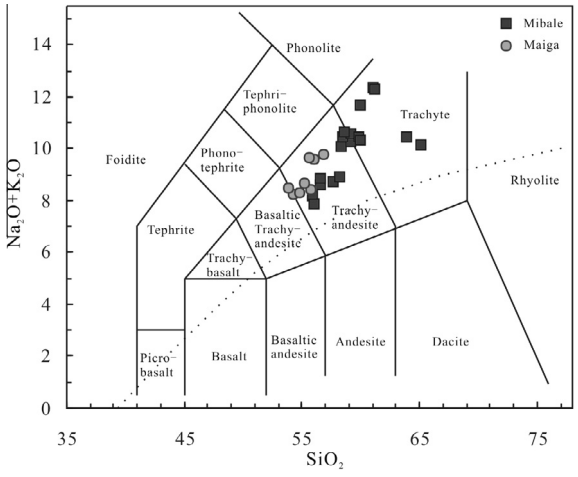

Fig. 3. TAS diagram (based on Bas et al., 1986) showing data for ultrapotassic rocks in Mibale and Maiga.

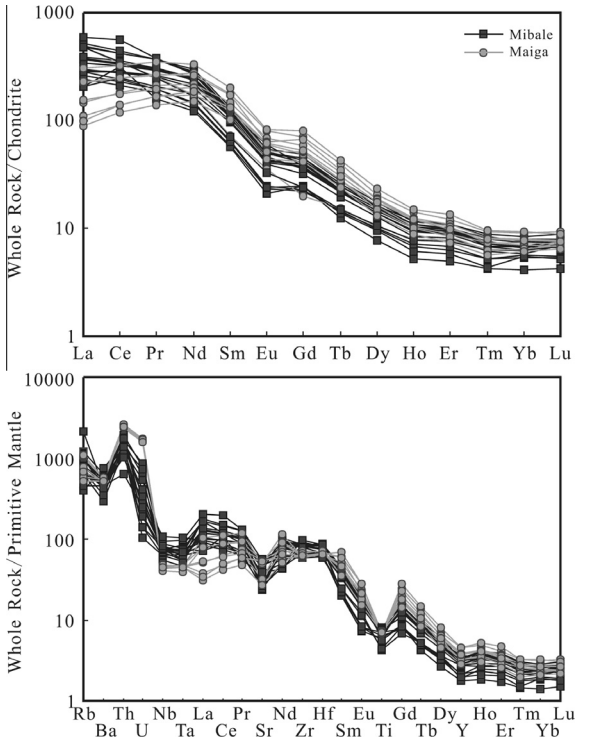

Fig. 4. REE and trace element concentrations in the Mibale and Maiga ultrapotassic rocks normalized to chondrite and primitive mantle after Sun and McDonough (1989).

respectively. The Mibale and Maiga ultrapotassic rocks have extremely unradiogenic Nd isotopes (Table 2), and $\varepsilon_{Nd}(t)$ values in the two locations range from −12.12 to −16.17. The Nd model ages (T_{DM}) range from 1.97 to 2.05 Ga, which lies within the range of values reported previously (1.3–2.9 Ga; Turner et al., 1996; Miller et al., 1999; Williams et al., 2004; Wang et al., 2008; Zhao et al., 2009; Guo et al., 2013; Liu et al., 2014b).

4.4. Re–Os isotopes

Whole-rock Re–Os isotope data and age-corrected Os isotopic ratios of the studied rocks are given in Table 3. The concentrations of Re and Os in the Mibale ultrapotassic rocks vary from 57.29 to 283.39 ppt and 14.32 to 82.47 ppt, respectively. The Re/Os ratios vary from 0.73 to 4.25. The initial ^{187}Os/^{188}Os ratios lie within the relatively wide range of 0.1550–0.1983. The Os model ages (T_{MA}), calculated relative to chondrite (Shirey and Walker, 1998), vary from 75 to 541 Ma. The $\gamma_{Os}(t)$ values of these ultrapotassic rocks range from 18.6 to 56.2.

The Re and Os concentrations in the Maiga ultrapotassic rocks are 53.78–234.76 ppt and 105.18–152.86 ppt, respectively, higher than in the Mibale ultrapotassic rocks. The Re/Os ratios are 0.47–2.23, and the initial ^{187}Os/^{188}Os ratios vary from 0.1370 to 0.1540, lower than in the Mibale ultrapotassic rocks. The values of T_{MA} are similar to those for Mibale, varying from 159 to 468 Ma, and the $\gamma_{Os}(t)$ values are 8.0–21.3.

Table 2
Sr–Nd isotopic composition of the ultrapotassic rocks in Mibale and Maiga, southern Tibet.

Samples	Location	Rb (ppm)	Sr (ppm)	$^{87}Rb/^{86}Sr$	$^{87}Sr/^{86}Sr \pm 2\sigma$	$^{87}Sr/^{86}Sr_i$	Sm (ppm)	Nd (ppm)	$^{147}Sm/^{144}Nd$	$^{143}Nd/^{144}Nd \pm 2\sigma$	$^{143}Nd/^{144}Nd_i$	$\varepsilon_{Nd}(t)$	T_{DM}(Ga)
CM10-04-04*	Mibale	753.9	838.8	2.6	0.719233 ± 14	0.719200	20.13	138.1	0.09	0.511958 ± 7	0.511957	−12.95	1.98
CM10-04-08	Mibale	604.1	984.5	1.8	0.719124 ± 19	0.719101	18.53	128.6	0.09	0.511952 ± 5	0.511951	−13.08	1.97
CM10-04-12*	Mibale	504.3	999.8	1.5	0.719610 ± 10	0.719591	14.62	82.07	0.11	0.511927 ± 6	0.511926	−13.56	2.00
CM10-04-14	Mibale	1335.1	556.1	7.0	0.722064 ± 13	0.721975	9.09	60.50	0.09	0.511894 ± 6	0.511893	−14.20	1.98
CM10-04-20	Mibale	403	786.2	1.5	0.720573 ± 10	0.720554	10.94	80.05	0.08	0.511927 ± 6	0.511926	−13.56	1.97
CM10-04-26	Mibale	450.8	997.4	1.3	0.720746 ± 14	0.720730	10.79	78.32	0.08	0.512000 ± 7	0.512000	−12.12	1.97
CQQ4-04-02	Maiga	368.8	1167.2	0.9	0.722189 ± 12	0.721971	26.83	127.9	0.13	0.511801 ± 7	0.511787	−16.17	2.03
CQQ4-04-03	Maiga	327.1	1165.7	0.8	0.722129 ± 13	0.721935	22.70	100.8	0.14	0.511835 ± 7	0.511820	−15.54	2.05

$\varepsilon_{Nd}(t) = (^{143}Nd/^{144}Nd_{sample}/^{143}Nd/^{144}Nd_{CHUR} - 1) \times 10{,}000$, $T_{DM} = \ln[1+(^{143}Nd/^{144}Nd_{sample}\text{-}^{143}Nd/^{144}Nd_{DM})/(^{147}Sm/^{144}Nd_{sample}\text{-}^{147}Sm/^{144}Nd_{DM})]/\lambda_{Sm}$.
In the calculation, $^{143}Nd/^{144}Nd_{CHUR} = 0.512638$, $^{147}Sm/^{144}Nd_{CHUR} = 0.1976$, $^{143}Nd/^{144}Nd_{DM} = 0.51315$, $^{147}Sm/^{144}Nd_{DM} = 0.2136$, $\lambda_{Sm} = 6.54 \times 10^{-12}$ year^{-1}.
The ages (t) in Mibale and Maiga ultrapotassic rocks are 12.5 Ma and the average ages of Maiga ultrapotassic rocks on Table 1, respectively.
* Data from Chen et al. (2012a).

Table 3
Re–Os isotopic composition of the ultrapotassic rocks in Mibale and Maiga, southern Tibet.

Samples	Location	Re (ppt)	2σ	Os (ppt)	2σ	$^{187}Re/^{188}Os$	2σ	$^{187}Os/^{188}Os$	2σ	$^{187}Os/^{188}Os_i$	$\gamma Os(t)$	T_{MA}(Ma)
CM10-04-02	Mibale	66.07	0.04	36.81	0.10	9.48	0.01	0.1600	0.0009	0.1580	24.5	201
CM10-04-04	Mibale	63.76	0.03	55.41	0.37	5.57	0.00	0.1691	0.0014	0.1679	32.3	460
CM10-04-08	Mibale	62.72	0.03	41.35	0.16	8.01	0.00	0.1673	0.0014	0.1657	30.5	298
CM10-04-10	Mibale	68.23	0.07	39.19	0.25	9.19	0.01	0.1756	0.0034	0.1736	36.8	314
CM10-04-12	Mibale	60.07	0.05	82.47	0.43	3.85	0.00	0.1558	0.0008	0.1550	22.1	459
CM10-04-14	Mibale	63.47	0.05	64.58	0.85	5.19	0.00	0.1727	0.0047	0.1716	35.2	541
CM10-04-17	Mibale	62.67	0.05	18.91	0.12	17.50	0.01	0.1791	0.0030	0.1754	38.2	174
CM10-04-20	Mibale	68.28	0.06	18.80	0.10	19.18	0.02	0.1922	0.0363	0.1882	48.3	200
CM10-04-24	Mibale	61.07	0.04	17.65	0.09	18.27	0.01	0.1651	0.0026	0.1613	27.1	119
CM10-04-26*	Mibale	283.39	0.05	66.66	23.14	20.54	0.00	0.1549	0.0002	0.1506	18.6	75
CM10-04-29*	Mibale	57.29	0.03	14.32	0.16	21.12	0.01	0.2027	0.0067	0.1983	56.2	212
CQQ4-04-03*	Maiga	53.78	0.10	114.93	0.54	2.47	0.00	0.1377	0.0006	0.1370	8.0	238
CQQ4-04-06*	Maiga	103.97	0.15	152.86	1.76	3.29	0.04	0.1519	0.0018	0.1510	19.0	468
CQQ4-04-10*	Maiga	234.76	0.62	105.18	0.23	10.79	0.04	0.1570	0.0004	0.1540	21.3	159

$\gamma_{Os}(t) = (^{187}Os/^{188}Os_{sample}/^{187}Os/^{188}Os_{chondrite} - 1) \times 100$, $T_{MA} = \ln[1 + (^{187}Os/^{188}Os_{Chondrite} - ^{187}Os/^{188}Os_{sample})/(^{187}Re/^{188}Os_{Chondrite} - ^{187}Re/^{188}Os_{sample})]/\lambda_{Re}$.
In the calculation, $^{187}Os/^{188}Os_{chondrite} = 0.1296$, $^{187}Re/^{188}Os_{chondrite} = 0.435$, $\lambda_{Re} = 1.666 \times 10^{-11}$ year^{-1}.
The ages (t) in Mibale and Maiga ultrapotassic rocks are 12.5 Ma and the average ages of Maiga ultrapotassic rocks on Table 1, respectively.
* The samples are analyzed at GIGCAS, the others are conducted at JAMSTEC.

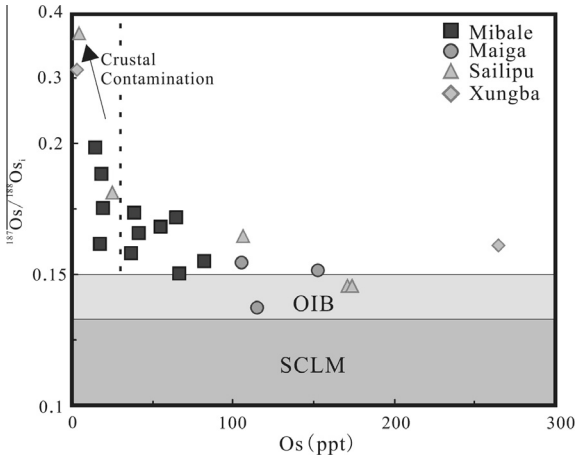

Fig. 5. Plot of Os vs initial $^{187}Os/^{188}Os$, showing the characteristics of the Mibale and Maiga ultrapotassic rocks (Sailipu and Xungba ultrapotassic rocks for comparison). See text for discussion of the possible crustal contamination. Data sources: Sailipu data from Wang et al. (2014); Xungba data from Schaefer et al. (2000); SCLM (sub-continental lithospheric mantle) data from Ellam et al. (1992), Meisel et al. (2001), Shirey and Walker (1998), Walker et al. (1989, 2002) and Widom and Shirey (1996); OIB data from Shirey and Walker (1998) and Xu et al. (2007).

The Re/Os ratios of the ultrapotassic rocks are all much higher than the value for fertile mantle ($^{187}Re/^{188}Os = 0.4$; Meisel et al., 1996; Shirey and Walker, 1998), and their Re and Os contents display negative and positive trends with increasing MgO contents, respectively (not shown), as expected for a melt, given the incompatibility of Re and the compatibility of Os. The initial $^{187}Os/^{188}Os$ ratios are 0.1370–0.1980, and samples with low Os concentrations display initial $^{187}Os/^{188}Os$ ratios that are obviously higher (Fig. 5).

5. DISCUSSION

5.1. Crustal contamination

The Mibale and Maiga ultrapotassic rocks all have relatively high initial $^{187}Os/^{188}Os$ ratios, which differs from typical lithosphere-derived melts (Fig. 5), and there are two main potential scenarios that could explain this: (1) their parental magmas were contaminated by crustal components during magma evolution (Esser and Turekian, 1993; Hattori et al., 2003), or (2) these ultrapotassic rocks inherited high $^{187}Os/^{188}Os$ ratios from their mantle source (Schaefer et al., 2000; Carlson and Nowell, 2001). The Mibale and Maiga rocks, combined with other ultrapotassic rocks from southern Tibet (e.g., samples from Sailipu and Xungba), show that samples with the lowest Os concentrations have distinctly high $^{187}Os/^{188}Os$ ratios (e.g., sample CM10-04-29, where Os = 14.32 ppt and $^{187}Os/^{188}Os = 0.1983$; Fig. 5, Table 3), suggesting that crustal materials were involved in the formation of the ultrapotassic magmas with low Os contents. The samples with low Os contents (e.g., CM10-04-17, CM10-04-20, CM10-04-24, and CM10-04-29) also have low MgO contents and high $^{187}Os/^{188}Os$ ratios, and they were possibly contaminated by crustal materials, and therefore cannot represent the initial magmas and sources (Xu et al., 2007). The Os isotopic data of these low-Os rocks will not be considered further in the following discussion on the mantle source of the ultrapotassic rocks in southern Tibet.

Excluding the samples with low Os contents, the Mibale and Maiga ultrapotassic samples with high Os contents (>30 ppt) display relatively homogeneous $^{187}Os/^{188}Os$ ratios, which is incompatible with crustal contamination. Furthermore, assuming that the parental magma had an initial $^{187}Os/^{188}Os = 0.125$ (Ellam et al., 1992), and that the crustal component from the Tibetan continental crust was characterized by $^{187}Os/^{188}Os = 1.1$ and Os = 30 ppt (Hattori et al., 2003), simple calculations show that a crustal component of ~50% must be added to the parental melt to reach the value of $^{187}Os/^{188}Os = 0.1983$. Given the large amounts of crust required to explain the $^{187}Os/^{188}Os$ ratios of the ultrapotassic rocks in southern Tibet, one would expect dramatically different major element contents to those observed (in particular the Mg# values should be much lower); consequently, such a high degree of crustal contamination appears to be unrealistic.

Crustal contamination is also excluded by the Nd and Sr isotopic compositions. Crustal contamination, particularly if accompanied by fractional crystallization, would have been expected to produce steeply positive correlations between Mg# values and $\varepsilon_{Nd}(t)$ values and a negative correlation between Mg# values and $^{87}Sr/^{86}Sr$ ratios. In fact, the Mibale and Maiga ultrapotassic rocks show the opposite correlations (Fig. 6), indicating that the Os–Nd–Sr isotopic characteristics were inherited in the parental magmas from the mantle source, rather than as a result of contamination by crustal materials. In addition, the ultrapotassic rocks in Mibale and Maiga display high K_2O contents and no correlation with Mg# variation (Fig. 6a), suggesting there were K-buffering minerals in their magmatic sources, such as phlogopite, which is widely appeared in the ultrapotassic rocks in southern Tibet (Turner et al., 1996; Miller et al., 1999; Guo et al., 2013).

There are many other lines of evidence that prove the ultrapotassic rocks with high Os contents are at most only slightly contaminated by crustal materials, including: (1) the Mibale and Maiga ultrapotassic rocks have high Mg# values (mean 67.8 and 75.1) and high MgO contents (generally >6 wt%), and such high-MgO ultrapotassic rocks probably represent the partial melts from a source in the mantle lithosphere (Prelević et al., 2012); (2) the ultrapotassic rocks have concentrations of incompatible elements that are many times higher than in crustal materials (Fig. 4), which render their Os–Nd–Sr isotopic systems relatively immune to contamination (Turner et al., 1996; Miller et al., 1999; Williams et al., 2004), and (3) the presence of mantle xenoliths and xenocrysts in the ultrapotassic rocks (Miller et al., 1999; Zhao et al., 2008; Liu et al., 2011, 2014a) testify to their rapid transport through the crust, further hinting that they were little contaminated by the crust, at least with regard to samples with high Os contents.

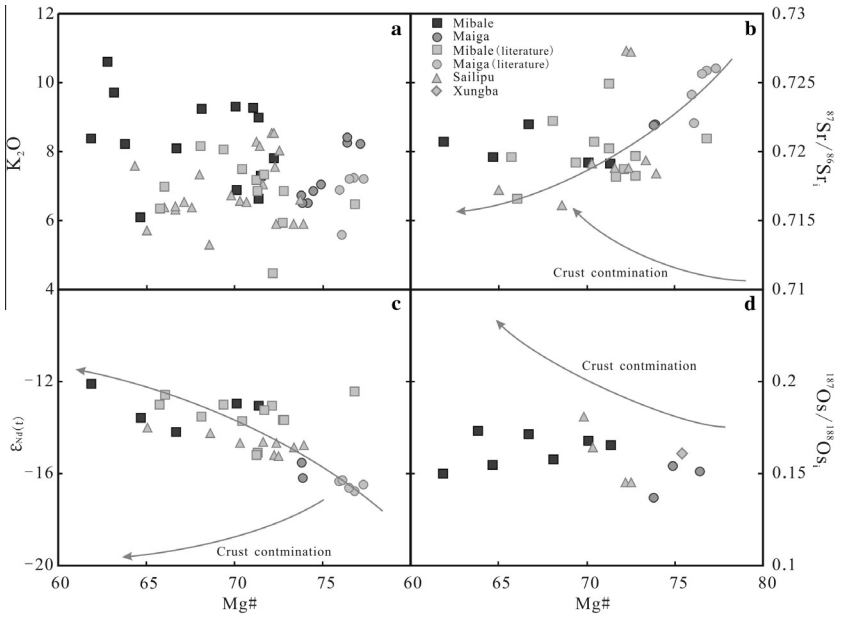

Fig. 6. Plots of K_2O contents and radiogenic isotopic composition vs Mg#, showing the trends of ultrapotassic rocks in southern Tibet. (a) K_2O vs Mg#. (b) Initial $^{87}Sr/^{86}Sr$ vs Mg#. (c) $\varepsilon_{Nd}(t)$ vs Mg#. (d) Initial $^{187}Os/^{188}Os$ vs Mg#. Data of the literature on ultrapotassic rocks of southern Tibet come from Chen et al. (2012a,b), Ding et al. (2006), Gao et al. (2007a,b), Guo et al. (2013), Schaefer et al. (2000), Wang et al. (2008, 2014), and Zhao et al. (2009).

5.2. Origin of radiogenic Os isotopic composition

The widespread high-MgO ultrapotassic rocks (MgO >6 wt%) provide good geochemical proxies for the post-collisional dynamics of orogenic lithospheric mantle (Foley et al., 1987; Prelević et al., 2012). In the case of the Miocene examples from southern Tibet (Chung et al., 2005; Chen, 2007; Gao et al., 2007b; Wang et al., 2014; Liu et al., 2014a,b), the ultrapotassic rocks are relatively homogeneous in their major, trace elements, and Nd–Sr isotopic compositions (Williams et al., 2004; Chen, 2007; Gao et al., 2007b; Wang et al., 2008, 2014; Zhao et al., 2009; Chen et al., 2012a,b; Liu et al., 2014b), indicating, as shown by Fig. 7a, that they were the products of partial melting, and that their radiogenic isotopic compositions probably represent those of the primary magmas.

Previous researchers have suggested these ultrapotassic rocks were derived from a metasomatized lithospheric mantle, based on their high potassium and trace elements concentrations (Turner et al., 1996; Miller et al., 1999; Williams et al., 2004; Chen et al., 2012a,b). Therefore, before constraining the source of these rocks, it is necessary to evaluate what could influence the Os isotopic compositions of these ultrapotassic rocks. During the process of partial melting, sulfides would affect the Os isotopic compositions of the ultrapotassic magmas, despite the insignificant volume of the sulfides (Hart and Ravizza, 1996; Harvey et al., 2010, 2011). Mass balance calculations for Os show

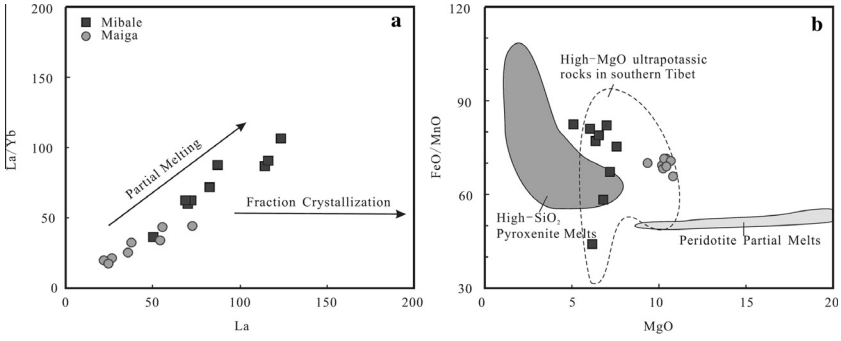

Fig. 7. Plot of major and trace element contents and ratios, showing the source characters of the ultrapotassic rocks from southern Tibet. (a) La vs La/Yb. (b) MgO vs FeO/MnO. Peridotite partial melt data are from Herzberg and Asimow (2008), high-SiO_2 pyroxenite melt data are from Pertermann and Hirschmann (2003), and the base figures is from Herzberg (2011).

that the bulk-rock Os in peridotite is dominated by contributions from two populations of sulfide grains: (1) interstitial metasomatic sulfides with low Os concentrations and radiogenic $^{187}Os/^{188}Os$ values, and (2) primary sulfides with high Os concentrations and unradiogenic $^{187}Os/^{188}Os$ values, preserved within the host silicate grains and shielded from interaction with transient melts and fluids (Harvey et al., 2010, 2011). The former would bring about a distinct increase in the $^{187}Os/^{188}Os$ ratios, while the latter would elevate the Os concentrations.

The $^{187}Re/^{188}Os$ ratios of interstitial sulfides are > 100, even up to 68000, which would lead to increases in the radiogenic Os compositions (Harvey et al., 2011). Given that Os and Re behave respectively as compatible and incompatible elements during partial melting of the mantle (Shirey and Walker, 1998), the $^{187}Re/^{188}Os$ ratios of rocks influenced by the presence of interstitial sulfides would be clearly much higher than those of the ultrapotassic rocks we have studied (2.5–21.1; Table 3). In addition, these interstitial sulfides that are preserved along the grain boundaries of the silicates possess generally supra-chondritic $^{187}Os/^{188}Os$ ratios (<0.37; Harvey et al., 2011). Mass balance calculations also show that a small volume of interstitial sulfides with low Os concentrations would not significantly change the Os isotopic compositions of their concomitant magmas (Harvey et al., 2010, 2011).

Based on the Os concentrations of mineral phases from natural rock samples, Hart and Ravizza (1996) noted that the partitioning of Os between olivine and basalt melt was 20 ± 5, and that for sulfides and basalt melt it was 2×10^6. Therefore, any sulfide precipitation from a basaltic melt will produce a horizontal trajectory on the plot of Os vs Ni concentrations (Hart and Ravizza, 1996). However, the data presented in this paper show a positive correlation between Os and Ni concentrations (not shown), which is obviously different from the situation with sulfide precipitation. Moreover, several earlier studies (Hart and Ravizza, 1996; Harvey et al., 2010) demonstrated a negligible contribution from the major rock-forming minerals (e.g., olivine, orthopyroxene, clinopyroxene, and spinel) to the Os concentrations of peridotite. Hence, the involvement of primary sulfides during the formation of the ultrapotassic magmas would have resulted in Os concentrations (>1 ppb; Harvey et al., 2011) obviously higher than those found.

The ultrapotassic rocks with high Os concentrations, as described in this paper, have initial $^{187}Os/^{188}Os$ ratios that are clearly higher than the values of mantle reservoirs (0.1276 for CHUR, 0.1296 for PUM, 0.126 for MORB-type mantle, 0.1–0.128 for SCLM, 0.123–0.1268 for DM; Walker et al., 1989, 2002; Ellam et al., 1992; Widom and Shirey, 1996; Hart et al., 1997; Shirey and Walker, 1998; Meisel et al., 2001; Gannoun et al., 2007). The OIB-like Os isotopic signatures of the ultrapotassic rocks from southern Tibet (e.g., the Sailipu, Xungba, Mibale, and Maiga areas; Fig. 5) show a clear depletion in HFSEs (e.g., Nb, Ta; Fig. 4), which is a typical imprint of lithospheric mantle that has been metasomatized by subduction-related agents. Moreover, the unradiogenic Nd isotopes of the ultrapotassic rocks exclude the possibility of a contribution from asthenospheric mantle. Therefore, although those samples with high Os contents have some OIB-like Os isotopic features, it is unlikely that they were derived from an OIB mantle source.

The mean Mg# values of the ultrapotassic rocks in the Mibale and Maiga areas are 67.8 and 75.1, and the average Ni concentrations are 156 and 357 ppm, respectively. These values seem paradoxical, and the enrichments in LILEs and radiogenic Sr–Nd isotopes signify derivation from a melt having an enriched component. To explain this problem, previous researchers proposed that primitive mantle (e.g., MORB or Indus-Yarlung Zangbo ophiolite-like lithospheric mantle) was metasomatized by melts/fluids derived from Indian continental sediments (Ding et al., 2003), or that Tethyan oceanic sediments (Gao et al., 2007b) contributed to the source of the ultrapotassic rocks in southern Tibet. However, metasomatism by melts and fluids derived from sediments would not have modified the radiogenic Os compositions significantly, because the Os content of sediments is much lower than that of the mantle (Shirey and Walker, 1998; Day et al., 2009), and it could only have significantly changed the concentrations of incompatible elements in the lithospheric mantle. Hence, it is reasonable to speculate that the ultrapotassic lavas have inherited their radiogenic Os isotopic compositions from a mantle source.

5.3. Source of the ultrapotassic magmas

There are mianly two potential sources for post-collisional ultrapotassic rocks: (1) a previously enriched lithospheric mantle (Turner et al., 1996; Miller et al., 1999; Williams et al., 2004; Liu et al., 2011) and (2) the Indian continental lithosphere (Ding et al., 2003; Gao et al., 2007b; Zhao et al., 2009). Although it is inevitable that the Indian continent would have had some impact on the southern Tibetan lithospheric mantle after the collision of India and Eurasia, there is no evidence that the Indian continent was the main contributor to the radiogenic Os isotopic compositions of the ultrapotassic rocks. Instead, we prefer to ascribe those compositions to a surviving ancient lithospheric mantle below southern Tibet, mainly on the basis of the following lines of evidence:

(1) Compared with the syn-collisional Linzizong Group volcanic rocks ($\varepsilon_{Nd}(t) = +5$ to -5; Mo et al., 2007, 2008) and the post-collisional adakitic rocks ($\varepsilon_{Nd}(t) = +3$ to -8; Chen et al., 2011; Hou et al., 2004; Guan et al., 2012; Guo et al., 2007), the widespread ultrapotassic rocks display relatively homogeneous unradiogenic Nd isotopic compositions ($\varepsilon_{Nd}(t) = -12$ to -17; Ding et al., 2003; Gao et al., 2007a,b; Liu et al., 2014b; Miller et al., 1999; Turner et al., 1996; Williams et al., 2004; Zhao et al., 2009; this study). If the subduction of the India continental lithosphere had indeed made a contribution to the formation of these ultrapotassic rocks, it would be difficult to explain how this process would have created such consistent values of $\varepsilon_{Nd}(t)$ in the ultrapotassic magmas.

(2) Previous researchers have attributed the unradiogenic Nd isotopes to the Higher Himalayan Crystalline Sequence (HHCS, the ancient basement of the Indian continent). However, the Nd and Sr isotopic compositions of the HHCS are highly heterogeneous ($^{87}Sr/^{86}Sr = 0.71–0.775$, $\varepsilon_{Nd}(t) = -8.1$ to -19; Ahmad et al., 2000; Richards et al., 2005). Therefore, the involvement of materials from the Indian continent should have given the ultrapotassic magmas variable elemental and isotopic compositions rather than the homogeneous compositions they actually possess.

(3) The Eocene volcanic rocks in southern Tibet have variable unradiogenic Nd isotope compositions ($\varepsilon_{Nd}(t)$ values low to -18; Lee et al., 2012), representing the remelting products of the basement of the Lhasa Terrane, which could not have had anything to do with the subduction of the Indian continent. Moreover, as a result of an investigation of inherited zircons in southern Tibet, Chu et al. (2006) and Zhu et al. (2011) concluded that an ancient crustal basement existed beneath the Lhasa Terrane.

(4) The widely distributed Miocene adakitic rocks occur along the IYZS, implying that the southern Tibetan crust had been thickened up to 50 km during the period from the Eocene to the Miocene (Chung et al., 2003, 2009; Hou et al., 2004; Gao et al., 2007a; Guan et al., 2012). This thickened crust would have prevented the subduction of the Indian continental lithosphere.

(5) The Re–Os model ages (75–541 Ma) of the ultrapotassic rocks analyzed in this study suggest that the lithospheric mantle in southern Tibet had been disturbed by multiple events before collision, and it seems, therefore, that a contribution from the Indian continental lithosphere to the formation of the ultrapotassic rocks was not essential.

(6) The consistency between the REE patterns of the ultrapotassic rocks and the model melts in equilibrium with clinopyroxenes in the mantle xenoliths in the Sailipu area (Liu et al., 2011) corroborates the suggestion that they had their sources in a metasomatized lithospheric mantle.

Although the India continental lithosphere cannot be excluded from having had an impact on the composition of the mantle beneath southern Tibet, any impact would have been restricted to the latest enrichment event. Therefore, the various Re–Os isotopic compositions of the ultrapotassic magmas were derived from an enriched mantle beneath southern Tibet, rather than from the subducted materials of the Indian lithosphere.

5.4. A pyroxenite-bearing lithospheric mantle?

The initial $^{187}Os/^{188}Os$ ratios of the ultrapotassic rocks described in this paper are obviously higher than those found in peridotite xenoliths worldwide ($\leqslant 0.1296$; Ellam et al., 1992; Meisel et al., 2001), suggesting that the partial melting of the latter could not have produced the Os isotopic composition of the former. This implies that another end-member component was involved. All these ultrapotassic rocks show high K_2O contents, testified the K-buffering (e.g. phlogopite) minerals were essential in the mantle source (Turner et al., 1996; Miller et al., 1999; Guo et al., 2013). Meanwhile, the least crustal-contaminated ultrapotassic rocks in southern Tibet have higher initial radiogenic Os ratios (>0.13), SiO_2 contents (>53 wt%), and lower MgO contents (Mibale area, 3.13–7.53 wt%; Maiga area, 9.33–10.75 wt%; Table A2) than typical peridotite-derived melts. An alternative interpretation is that the ultrapotassic rocks were the products of partial melting of a phlogopite pyroxenite-bearing lithospheric mantle (Foley, 1992; Schaefer et al., 2000; Carlson and Nowell, 2001; Conticelli et al., 2007; Sobolev et al., 2008). Such pyroxenite-derived melts would have relatively high K_2O, SiO_2 and low MgO contents (Sobolev et al., 2007), which is consistent with the results of our study.

It is generally accepted that pyroxenite have variable Os concentrations and high Os isotopic ratios (Shirey and Walker, 1998; Sobolev et al., 2008), and they are widespread in the lithospheric mantle. The Mibale and Maiga ultrapotassic rocks have high initial $^{187}Os/^{188}Os$ ratios, and they show affinities with a pyroxenite-bearing lithospheric mantle, as described by Schaefer et al. (2000), Carlson and Nowell (2001), and Sobolev et al. (2008). It should be noted that pyroxenite xenoliths have been found in ultrapotassic rocks from southern Tibet (Zhao et al., 2008; Liu et al., 2011), and this further supports that a pyroxenite-bearing lithosphere most likely exists below southern Tibet.

Olivine phenocrysts in most of the Sailipu xenoliths in southern Tibet have lower CaO (<0.1 wt%) and distinctly lower MnO (<0.16 wt%) contents than those of magmatic olivines, and they have high NiO contents (>0.13 wt%) (Liu et al., 2011). The ultrapotassic rocks of Mibale and Maiga also have high Ni concentrations and lower MnO contents (<0.1 wt%). Previous studies concluded that partial melts from pyroxenite would show enrichment in Ni and Si but depletion in Mg, Mn, and Ca compared with the peridotite-derived counterparts (Sobolev et al., 2005, 2007, 2008; Gurenko et al., 2009). Mixing between peridotite- and pyroxenite-derived melts would result in olivines with relatively high Ni but low Ca and Mn contents compared with the melts formed by peridotite partial melting.

The ultrapotassic rocks of southern Tibet have distinctly variable FeO/MnO ratios (Fig. 7b; assuming all the Fe_2O_3 is transformed into FeO, following Herzberg, 2011, and Pertermann and Hirschmann, 2003), and experiments on pyroxenite-derived melts produced a wide range of FeO/MnO ratios. In contrast, the FeO/MnO ratios in peridotite-derived melts are relatively constant because those melts cannot effectively fractionate Fe and Mn, and the FeO/MnO ratios are much lower than in pyroxenite-derived melts (Liu et al., 2008). All of these suggest that formation of the ultrapotassic rocks were involved the partial melting of a pyroxenite.

The ultrapotassic rocks in southern Tibet that have primitive features (MgO >6 wt%) mainly belong to the intermediate alkaline series (Fig. 3), whereas the results of melting experiments on anhydrous lherzolite show that the silica contents of a low-degree partial melt are <55 wt% (Baker et al., 1995). Melts from pyroxenite would have higher SiO_2 contents and be enriched in LILEs (Yaxley and Green, 1998; Sobolev et al., 2005, 2007, 2008). Moreover, Hirschmann et al. (2003) pointed out that alkalic magmas could be generated by partial melting of pyroxenite, which is in accord with the ultrapotassic rocks of southern Tibet. Therefore, the above arguments indicate that the ultrapotassic rocks of southern Tibet most probably involved a pyroxenite component in their magmatic source.

To determine the nature of the pyroxenite involved requires us to explain the Os isotopic data of the ultrapotassic rocks. Therefore, we performed some simple isotopic modeling based on a binary model (Fig. 8; Langmuir et al., 1978) where the primitive parental melt of the peridotite is assumed to have Os = 500 ppt and $^{187}Os/^{188}Os = 0.125$ (Ellam et al., 1992; Chesley et al., 2002), and the pyroxenite Os = 200 ppt and $^{187}Os/^{188}Os = 0.8$ (Day et al., 2009). The results indicate that <20% of pyroxenite in the lithospheric mantle would produce the radiogenic Os compositions of the ultrapotassic rocks of southern Tibet (Fig. 8). This result is reasonable because pyroxenite have a wide distribution in the lithospheric mantle (Hirschmann and Stolper, 1996; Becker et al., 2004; Liu et al., 2005; Day et al., 2009; Gurenko et al., 2009). In the mantle, veins or sheets of pyroxenite, enriched in incompatible elements, would have a lower melting temperature than the surrounding peridotite (Allegre and Turcotte, 1986; Hirschmann and Stolper, 1996; Hirschmann et al., 2003), and hybrids between melts

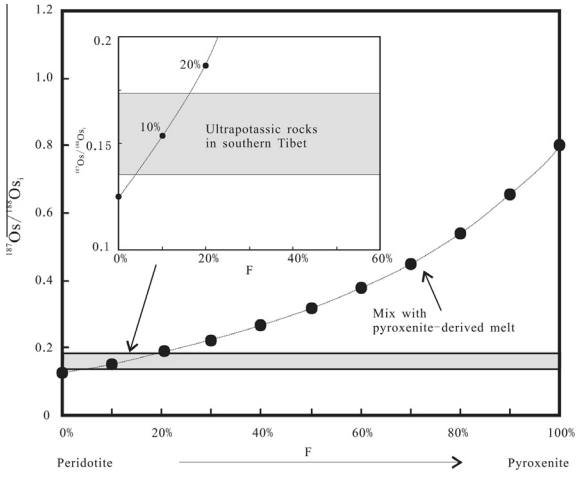

Fig. 8. Binary mixing between a hypothetical peridotite- and a pyroxenite-lithospheric mantle. The end-members composition used in the modeling are after Chesley et al. (2002), Ellam et al. (1992) and Day et al. (2009), and more details are given in the text. The Os isotopic data for the ultrapotassic rocks of southern Tibet are shown as the shaded area.

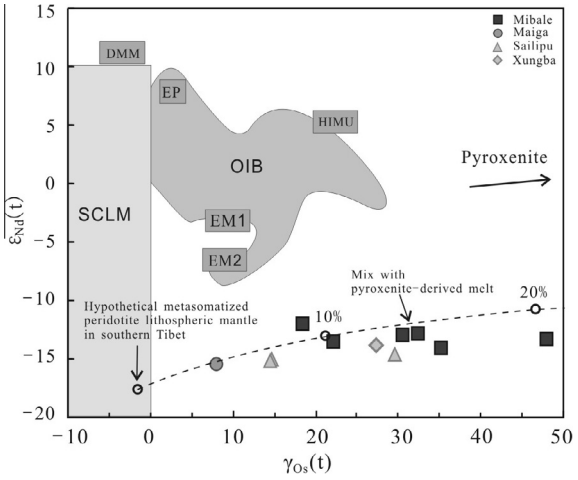

Fig. 9. Plot of $\gamma_{Os}(t)$ vs $\varepsilon_{Nd}(t)$ for the ultrapotassic rocks of southern Tibet. The mantle reservoirs and base figure are from Shirey and Walker (1998) and Xu et al. (2007). The Sailipu and Xungba ultrapotassic rocks are shown for comparison. Binary mixing between a hypothetical peridotite lithospheric mantle and a pyroxenite is also shown, and the end-members used in the modeling are from Chesley et al. (2002), Ellam et al. (1992) and Day et al. (2009). More details are given in the text.

of pyroxenite and peridotite would show these enrichment characteristics (Yaxley and Green, 1998; Liu et al., 2005).

In addition, in contrast to the fact that Rb-Sr isotopic systematics can be easily modified by fluids or melts, Nd is a strongly incompatible element that would not change its isotopic composition during the evolution of the magma. Consequently, the $\varepsilon_{Nd}(t)$ values, coupled with $\gamma_{Os}(t)$ values, will effectively identify the source of the ultrapotassic rock in southern Tibet. Then we assume the $\varepsilon_{Nd}(t)$ value (+5) and high Nd concentration (100 ppm) represent the pyroxenite-derived melt that existed in the southern Tibetan lithospheric mantle. With reference to the most metasomatized peridotite and enriched unradiogenic $\varepsilon_{Nd}(t)$ in the ultrapotassic rocks of southern Tibet (Turner et al., 1996; Miller et al., 1999; Ding et al., 2003; Williams et al., 2004; Chung et al., 2005; Zhao et al., 2006, 2009; Gao et al., 2007a,b; Guo et al., 2013; Liu et al., 2014b), we chose a $\varepsilon_{Nd}(t)$ value of −17 for peridotite-derived melt and a Nd content of 50 ppm. Combining the above radiogenic Os isotopic compositions, the currently existing radiogenic Os–Nd isotopic compositions are close to the mixing curve between melts of peridotite and pyroxenite (Fig. 9). The trends also indicate that <20% pyroxenite is required in the lithospheric mantle, and the results provide further support for the suggestion that pyroxenite played an essential role in the origin of the ultrapotassic rocks of southern Tibet.

5.5. Geodynamic implications

Previous studies have suggested several geodynamic models of post-collision in the southern Tibet, such as gravitational collapse, convective removal of the southern

Tibetan lithospheric mantle, and break-off of the Indian continental lithospheric slab, which could be related to the ultrapotassic–potassic and adakitic magmatic activity (Miller et al., 1999; Maheo et al., 2002; Williams et al., 2004; Chung et al., 2005; Liu et al., 2011). The small-volume ultrapotassic lavas could have originated from gravitational collapse of the lithospheric mantle. However, these ultrapotassic rocks are widely distributed in southern Tibet, and adakitic rocks and peraluminous granites also formed at the same time (Chung et al., 2003, 2009; Hou et al., 2004; Liao et al., 2007). The wide extent of this Miocene magmatism therefore requires a tectonic mechanism that involved the whole of southern Tibet rather than some specific locations. The ultrapotassic rocks were typically emplaced along a series of N-S grabens (Zhao et al., 2009), and the close temporal and spatial links between the grabens (24–10 Ma; Blisniuk et al., 2001; Royden et al., 2008) and the magmatism (26–8 Ma; Zhao et al., 2009; Guo et al., 2013; Liu et al., 2013, 2014b) indicates that the Tibetan Plateau underwent a transition from compression to extension during the early Miocene. The eruptive Mibale and Maiga ultrapotassic magmatism is therefore probably the result of Miocene extension in the southern Tibetan region (Chen, 2007).

It is generally thought that the Os model ages could represent the time of magma separation from the mantle, and the start of developments that are in accordance with chondritic evolution (Shirey and Walker, 1998), because there is substantial Re/Os fractionation during magmatic extraction. Therefore, the Os model ages described in this paper probably represent the time of multiple magmatic events and Os depletion of both pyroxenite and peridotite in southern Tibet. Re–Os isotopic compositions of the Mibale and Maiga ultrapotassic rocks, coupled with their geochemical characteristics, indicate the existence of pyroxenite with relatively radiogenic Os isotopes in the lithospheric mantle. The formation of the pyroxenite could have been related to the subduction of the Paleozoic Tethys and Neo-Tethys Oceans. This earlier oceanic crustal subduction would have provided incompatible elements (e.g., Re, LILEs) back into the southern Tibetan lithospheric mantle, and after a long time of radiogenic daughter growth this would have led to relatively high radiogenic Os and Sr isotopic compositions and unradiogenic Nd isotopic characteristics.

Thus, here we favor the concepts of the convective removal of lithospheric mantle or continental lithospheric slab break-off as the possible causes of the ultrapotassic rocks in southern Tibet. Both mechanisms would have led to regional extension (Turner et al., 1996; Chung et al., 2005) and partial melting of widespread pyroxenite in the lithospheric mantle as veins or sheets (Foley, 1992; Carlson and Nowell, 2001). The radiogenic Os and unradiogenic Nd compositions of the ultrapotassic lavas were derived from hybrid melts of pyroxenite and perodotite in an ancient lithospheric mantle beneath southern Tibet, during a process that took place during convective removal or break-off of the lithospheric mantle.

6. CONCLUSIONS

(1) The Mibale ultrapotassic rocks were erupted at 12.5 Ma, which is coincident with the transformation of the Tibetan Plateau from a compressive to an extensional tectonic regime. The ultrapotassic rocks are therefore probably related to Miocene post-collision regional extension in southern Tibet.
(2) The initial Os isotopic compositions of the ultrapotassic rocks are higher than those of the peridotite xenoliths from the lithospheric mantle. Combined with the elemental geochemical characteristics, this suggests that the generation of the ultrapotassic rocks of southern Tibet can be attributed to a phlogopite pyroxenite-bearing lithospheric mantle source.
(3) Other Miocene magmatic activity that is related to the ultrapotassic–potassic rocks, including the development of adakitic rocks and peraluminous granites in southern Tibet, is consistent with a genetic model that involves the convective removal or break-off of lithospheric mantle.

ACKNOWLEDGEMENTS

We thank two anonymous reviewers for their constructive and thoughtful reviews which greatly revise and improve the manuscript. Drs. Marc Norman and Wei-Dong Sun are thanked for their helpful comments and editorial handing. Feng Huang thanks Drs. Xiao-Wei Li, Lin Ma and Jie-Qiong Zou for their constructive discussions in improving an early manuscript. We thank Dr. Katsuhiko Suzuki for his help in Re–Os isotopic analyses at JAMSTEC and Ping Jian for help in SHRIMP II analyses at Beijing. This research was supported by the Strategic Priority Research Program (B) of Chinese Academy of Sciences (XDB03010300), the Major State Basic Research Program of the People's Republic of China (2015CB452602), the Natural Science Foundation of China (41373030, 41273039, and 41121002), GIGCAS 135 project to Ji-Feng Xu (Y234021002) and the IGCP project (IGCP/SIDA-600). This is GIGCAS contribution No. IS-2059.

APPENDIX .

Table A1
SHRIMP U–Pb data of zircons from sample CM10-04-03 in Mibale, southern Tibet.

	U/ppm	Th/ppm	Th/U	Pb^*/ppm	f_{206}	Isotopic ratios						Ages						^{207}Pb correct ratios and ages			
						$^{207}Pb/^{235}U$	1σ	$^{206}Pb/^{238}U$	1σ	$^{207}Pb/^{206}Pb$	1σ	$^{207}Pb/^{235}U$	1σ	$^{206}Pb/^{238}U$	1σ	$^{207}Pb/^{206}Pb$	1σ	$^{206}Pb/^{238}U$	1σ	$^{206}Pb/^{238}U$	1σ
CM10-04-03-1	293	918	3.13	1	0.12	0.0231	0.0135	0.0022	0.0003	0.0764	0.0419	23.21	13.5	14.14	2.04	1104.3	1854	0.0021	0.0003	13.6	1.9
CM10-04-03-2	355	1249	3.52	1	0.24	−0.0056	−0.0173	0.0018	0.0003	−0.0232	0.0722	0	0	11.26	1.6	0	0	0.0019	0.0002	12.2	1.3
CM10-04-03-3	93	196	2.10	0	0.36	0.0879	0.1008	0.0025	0.0010	0.2541	0.2618	85.58	89.93	16.16	6.28	3210.7	3211	0.0019	0.0003	11.9	2.1
CM10-04-03-4	122	396	3.25	1	0.38	0.0352	0.0498	0.0022	0.0006	0.1141	0.1546	35.1	47.68	14.4	3.9	1864.9	1865	0.0020	0.0004	13.2	2.3
CM10-04-03-5	170	117	0.69	2	0.07	0.0928	0.0742	0.0111	0.0010	0.0607	0.0475	90.12	71.36	71.13	6.48	627.48	5717	0.0109	0.0008	70	5.4
CM10-04-03-6	30	41	1.35	1	0.15	0.3671	0.5279	0.0258	0.0286	0.1031	0.0817	317.47	331.6	164.43	176.9	1679.7	4038	0.0241	0.0266	153.6	159
CM10-04-03-7	336	922	2.74	1	0.10	0.0360	0.0256	0.0022	0.0004	0.1190	0.0801	35.88	25.4	14.11	2.29	1941.9	2362	0.0020	0.0003	12.8	1.8
CM10-04-03-8	90	65	0.72	1	0.23	−0.0316	−0.1989	0.0080	0.0023	−0.0285	0.1805	0	0	51.56	14.94	0	0	0.0088	0.0014	56.5	8.9
CM10-04-03-9	490	1059	2.16	2	0.13	0.0260	0.0160	0.0022	0.0003	0.0873	0.0510	26.06	15.96	13.9	1.85	1367.7	1976	0.0021	0.0003	13.2	1.6
CM10-04-03-10	388	1400	3.61	2	0.21	0.0260	0.0216	0.0020	0.0003	0.0927	0.0742	26.04	21.65	13.1	1.97	1480.8	4484	0.0019	0.0002	12.3	1.5
CM10-04-03-11	135	333	2.47	0	0.24	0.0029	0.0248	0.0020	0.0003	0.0102	0.0884	2.89	24.8	13.08	1.76	0	0	0.0021	0.0002	13.7	1.2
CM10-04-03-12	175	472	2.69	1	0.09	0.0985	0.0256	0.0028	0.0003	0.2515	0.0569	95.36	23.97	18.28	1.89	3194.2	412.8	0.0021	0.0002	13.5	1.4
CM10-04-03-13	165	413	2.51	0	0.40	−0.0151	−0.0328	0.0018	0.0004	−0.0608	0.1331	0	0	11.61	2.68	0	0	0.0021	0.0003	13.2	1.8
CM10-04-03-14	1199	3625	3.02	4	0.11	0.0019	0.0080	0.0018	0.0002	0.0076	0.0320	1.92	8.08	11.64	1.08	0	0	0.0019	0.0002	12.2	1.1
CM10-04-03-15	870	2276	2.62	2	0.26	−0.0063	−0.0105	0.0018	0.0002	−0.0255	0.0428	0	0	11.55	1.12	0	0	0.0020	0.0002	12.6	1
CM10-04-03-16	283	888	3.13	1	0.18	0.0099	0.0269	0.0022	0.0003	0.0332	0.0898	9.96	26.68	13.87	1.93	0	0	0.0022	0.0002	14.1	1.1
CM10-04-03-17	746	1739	2.33	2	0.19	−0.0110	−0.0123	0.0019	0.0002	−0.0433	0.0487	0	0	11.9	1.51	0	0	0.0021	0.0003	13.3	1.6
CM10-04-03-18	348	1305	3.75	1	0.30	0.0091	0.0239	0.0018	0.0003	0.0375	0.0976	9.19	23.79	11.33	1.93	0	0	0.0018	0.0002	11.1	1.5
CM10-04-03-19	442	1098	2.48	1	0.06	0.0201	0.0124	0.0018	0.0002	0.0835	0.0497	20.24	12.45	11.26	1.19	1281.1	2087	0.0017	0.0002	10.7	1
CM10-04-03-20	343	1478	4.31	1	0.52	−0.0713	−0.0366	0.0014	0.0004	−0.3815	0.1792	0	0	8.74	2.38	0	0	0.0021	0.0003	13.5	1.7
CM10-04-03-21	351	1028	2.92	1	0.25	0.0084	0.0215	0.0019	0.0003	0.0318	0.0807	8.48	21.43	12.32	2.14	0	0	0.0020	0.0003	12.5	1.8
CM10-04-03-22	269	549	2.04	1	0.06	0.0499	0.0309	0.0021	0.0003	0.1729	0.1004	49.43	30.31	13.47	2.07	2586.1	1585	0.0018	0.0002	11.3	1.2
CM10-04-03-23	2180	13095	6.01	10	0.04	0.0107	0.0048	0.0019	0.0001	0.0417	0.0183	10.8	4.85	11.98	0.77	0	0	0.0019	0.0001	12.1	0.7
CM10-04-03-24	152	288	1.89	0	0.36	−0.0171	−0.0377	0.0018	0.0004	−0.0687	0.1527	0	0	11.61	2.74	0	0	0.0021	0.0002	13.3	1.2
CM10-04-03-25	102	235	2.30	1	0.23	0.1119	0.0589	0.0024	0.0004	0.3365	0.1629	107.69	55.26	15.53	2.4	3646.9	1055	0.0015	0.0005	9.8	3.4

Pb^* = whole Pb concentrations, f_{206} represents the percentage of the common ^{206}Pb in the whole Pb concentrations.

Table A2
Major (wt%) and trace (ppm) element data of the ultrapotassic rocks in Mibale and Maiga, southern Tibet.

Samples	CM10-04-02	CM10-04-04*	CM10-04-05	CM10-04-08	CM10-04-10	CM10-04-12*	CM10-04-14	CM10-04-15	CM10-04-17	CM10-04-19
Location	Mibale	Mibale	Mibale	Mibale	Mibale	Mibale	Mibale	Mibale	Mibale	Mibale
Roke type	trachy-andesite	trachyte	trachy-andesite	trachy-andesite	trachy-andesite	trachy-andesite	trachyte	trachyte	trachy-andesite	trachyte
SiO_2	59.84	56.63	57.64	55.95	58.34	55.99	59.99	59.97	56.61	61.00
TiO_2	1.40	1.66	1.75	1.69	1.62	1.56	1.50	1.31	1.49	1.28
Al_2O_3	13.13	10.83	11.49	11.04	13.82	11.10	13.01	14.12	11.92	13.82
Fe_2O_3T	4.11	6.07	5.15	5.99	5.66	7.53	4.45	4.61	6.01	4.20
MnO	0.05	0.08	0.08	0.07	0.06	0.08	0.05	0.07	0.13	0.06
MgO	4.44	7.18	6.76	7.53	5.03	6.96	4.50	4.00	6.13	3.57
CaO	3.36	5.49	5.18	5.61	4.09	5.84	3.57	3.21	6.16	2.95
Na_2O	1.21	1.75	0.91	1.56	1.86	1.77	2.25	1.94	1.92	1.77
K_2O	9.24	6.89	7.80	6.63	8.23	6.11	8.10	9.72	6.94	10.61
P_2O_5	0.07	0.30	0.12	0.55	0.16	0.08	0.07	0.07	0.41	0.03
LOI	2.6	3.1	2.7	3.1	1.1	2.5	2.4	0.7	2.4	0.6
Total	99.40	99.96	99.63	99.67	99.96	99.49	99.83	99.74	100.09	99.92
Mg#	68.1	70.1	72.2	71.4	63.8	64.7	66.7	63.2	66.9	62.8
Cr	215	396.1	455	360.4	220.9	449.6	260.8	146.9	343.5	105.9
Co	14.5	24.0	23.2	22.7	19.8	30.4	15.3	15.5	35.7	10.8
Ni	119	210.4	227.8	213.3	145.2	215.2	137.8	101.5	194.5	65.87
Sc	12.0	17.3	21.5	26.9	17.5	22.2	22.9	22.5	24.5	25.6
V	100.9	103.9	136.1	115.8	107.1	146.6	113.8	48.4	154	85.6
Rb	291.2	753.9	252.9	604.1	641.9	504.3	1335.1	366.4	438.4	411.8
Sr	522.7	838.8	623.3	984.5	1200.8	999.8	556.1	1165.4	1083.7	800.3
Ba	3175.8	4465.3	5216.7	3881.1	2867.9	3626.3	3038.6	3987.5	3564.2	3120.5
Nb	61.9	53.2	55.6	52.0	39.5	52.7	52.2	65.6	50.0	54.9
Ta	3.1	3.5	2.9	2.3	1.9	3.0	2.6	3.9	2.7	2.6
Zr	911.2	952.5	919.6	885.9	779.7	740.5	738.9	931.8	752.7	901.4
Hf	23.5	26.9	25.4	20.9	18.4	20.5	20.0	25.9	20.4	19.8
Y	8.6	15.0	13.7	16.2	15.4	12.8	9.9	14.0	15.0	8.2
Th	88.3	117.9	123.9	108.4	133.1	165.9	85.6	148.2	145.2	54.0
U	6.2	4.1	3.0	5.1	12.8	16.3	5.8	4.9	18.0	5.2
Pb	74.6	67.8	83.0	57.2	71.4	77.9	44.3	91.0	111.9	51.9
La	61.57	113.61	115.61	122.96	69.31	49.65	57.83	139.76	90.25	49.28
Ce	140.70	260.20	257.50	269.90	174.50	153.40	129.80	344.90	208.30	190.20
Pr	18.66	34.78	34.74	35.32	24.85	19.60	17.07	35.77	28.82	15.09
Nd	68.06	138.10	131.90	128.60	102.70	82.07	60.50	126.80	112.40	57.46
Sm	9.93	20.13	19.45	18.53	17.14	14.62	9.09	18.06	18.61	8.82
Eu	1.42	3.16	2.87	2.92	3.45	2.37	1.35	2.94	2.84	1.22
Gd	4.63	9.90	9.18	8.30	7.75	7.66	4.60	8.69	9.21	5.11
Tb	0.54	1.03	0.92	0.86	0.82	0.83	0.54	0.93	0.97	0.47
Dy	2.58	4.48	4.15	3.91	3.70	3.67	2.47	3.96	4.13	1.97
Ho	0.40	0.65	0.62	0.58	0.57	0.57	0.38	0.61	0.66	0.30
Er	1.14	1.81	1.65	1.61	1.55	1.62	1.05	1.64	1.82	0.83
Tm	0.14	0.22	0.20	0.17	0.19	0.21	0.13	0.19	0.22	0.11
Yb	0.95	1.30	1.27	1.15	1.15	1.36	0.90	1.16	1.41	0.70
Lu	0.14	0.20	0.19	0.17	0.18	0.20	0.14	0.20	0.22	0.11

Table A2 (*continued*)

Samples	CM10-04-20	CM10-04-21	CM10-04-22	CM10-04-24	CM10-04-26	CM10-04-27	CM10-04-28	CM10-04-29	CQQ4-04-01	CQQ4-04-02
Location	Mibale	Mibale	Mibale	Mibale	Mibale	Mibale	Mibale	Mibale	Maiga	Maiga
Roke type	trachyte	trachy-andesite	trachy-andesite	trachyte	trachyte	trachy-andesite	trachy-andesite	trachy-andesite	trachy-andesite	trachy-andesite
SiO_2	65.17	58.17	59.10	61.15	63.89	58.52	59.15	58.60	55.70	54.32
TiO_2	0.93	1.45	1.62	1.21	0.94	1.63	1.65	1.63	1.55	1.52
Al_2O_3	13.41	12.30	11.19	14.17	13.67	11.72	12.02	11.48	11.37	11.57
Fe_2O_3T	3.66	4.85	5.04	4.30	3.82	5.25	5.11	5.34	6.98	7.27
MnO	0.05	0.10	0.06	0.06	0.06	0.06	0.06	0.06	0.09	0.09
MgO	2.94	6.14	6.35	3.61	3.13	6.50	6.03	6.11	10.11	10.36
CaO	2.51	5.69	4.13	2.53	2.60	4.13	3.90	4.20	5.01	5.33
Na_2O	2.48	1.62	1.27	2.04	2.06	1.18	1.27	1.30	1.94	1.71
K_2O	7.68	7.30	8.97	10.29	8.39	9.27	9.31	9.36	6.50	6.51
P_2O_5	0.04	0.26	0.11	0.07	0.05	0.09	0.06	0.13	0.14	0.33
LOI	0.7	2.0	1.7	0.4	1.3	1.1	1.2	1.4	0.9	1.3
Total	99.61	99.88	99.52	99.82	99.93	99.47	99.70	99.62	100.24	100.32
Mg#	61.4	71.5	71.4	62.4	61.9	71.0	70.0	69.4	74.1	73.9
Cr	117.5	332.8	366.4	101.8	116.7	350.7	364.5	359	728.9	704.8
Co	11.9	27.6	19.9	13.1	12.7	23.0	19.2	22.4	18.4	16.1
Ni	74.24	121.2	194.3	75.7	74.51	217.3	187	231.4	305	370.5
Sc	24.9	21.7	18.1	23.9	17.7	18.5	16.2	18.5	21.9	20.7
V	73.0	151.3	123.3	78.4	72.4	122.8	123.2	116.1	154.7	144.1
Rb	403	368.1	590.9	457.9	450.8	516.9	488.4	629.6	381.3	368.8
Sr	786.2	1112.2	507.4	819.4	997.4	565.3	491.4	528.4	1152.4	1167.2
Ba	2065.1	3605.8	3695.2	2969.6	2427.9	3334.3	3394.7	3334.9	3737.1	3907.6
Nb	53.7	53.3	45.1	75.5	59.1	43.8	46.8	48.7	32.2	33.0
Ta	3.1	2.8	2.7	4.2	2.8	2.2	2.4	2.2	1.9	2.0
Zr	663.8	789.7	925.1	1097.4	773.5	929.6	964	1009.5	685.5	688.6
Hf	18.4	20.2	26.7	26.3	17.8	23.0	25.7	25.1	20.7	20.6
Y	9.5	13.0	12.1	8.8	12.3	12.3	12.7	14.3	14.7	21.0
Th	104.9	152.1	107.0	122.2	118.4	97.3	115.8	113.4	201.7	212.8
U	11.1	6.7	2.2	7.0	15.3	3.0	4.0	8.7	33.8	34.5
Pb	129.9	95.5	54.2	57.0	137.3	34.8	46.9	50.8	103.0	104.1
La	113.30	71.42	67.98	66.38	114.35	86.66	81.67	92.31	26.05	53.66
Ce	210.80	170.20	174.20	148.50	211.50	200.80	198.00	221.30	86.04	153.70
Pr	24.05	24.08	25.20	18.65	23.82	28.06	27.75	29.43	16.11	25.18
Nd	80.05	94.58	101.30	67.05	78.32	108.90	113.10	117.10	80.11	127.90
Sm	10.94	15.21	16.26	9.76	10.79	16.26	17.27	18.41	19.07	26.83
Eu	2.09	2.48	2.42	1.41	1.89	2.28	2.52	2.67	3.46	4.61
Gd	4.06	7.69	8.05	5.08	4.88	6.55	7.60	7.34	10.07	14.63
Tb	0.57	0.82	0.83	0.52	0.56	0.73	0.80	0.82	1.04	1.48
Dy	2.62	3.66	3.56	2.43	2.67	3.21	3.56	3.56	4.08	5.23
Ho	0.45	0.57	0.53	0.34	0.44	0.48	0.54	0.55	0.59	0.80
Er	1.28	1.53	1.47	0.96	1.27	1.35	1.51	1.58	1.48	1.98
Tm	0.17	0.18	0.17	0.11	0.16	0.16	0.19	0.19	0.19	0.24
Yb	1.07	1.14	1.08	0.93	1.07	0.99	1.13	1.20	1.18	1.55
Lu	0.19	0.21	0.18	0.13	0.17	0.18	0.19	0.18	0.17	0.24

Table A2 (*continued*)

Samples	CQQ4-04-03	CQQ4-04-04	CQQ4-04-05	CQQ4-04-06	CQQ4-04-09	CQQ4-04-10
Location	Maiga	Maiga	Maiga	Maiga	Maiga	Maiga
Roke type	trachy-andesite	trachy-andesite	trachy-andesite	trachy-andesite	trachy-andesite	trachy-andesite
SiO_2	54.83	53.82	56.00	55.64	56.89	55.20
TiO_2	1.52	1.47	1.46	1.53	1.52	1.52
Al_2O_3	11.45	11.31	11.26	11.28	11.45	11.33
Fe_2O_3T	7.20	7.30	6.27	6.24	5.71	6.90
MnO	0.09	0.10	0.08	0.08	0.07	0.09
MgO	10.24	10.75	10.66	10.21	9.33	10.38
CaO	5.12	5.04	4.14	4.00	3.92	4.54
Na_2O	1.58	1.62	1.38	1.38	1.38	1.64
K_2O	6.74	6.84	8.23	8.27	8.42	7.03
P_2O_5	0.19	0.55	0.42	0.24	0.12	0.11
LOI	1.2	1.1	0.5	0.8	1.2	1.1
Total	100.16	99.88	100.37	99.68	99.98	99.84
Mg#	73.8	74.5	77.1	76.4	76.4	74.9
Cr	677.4	582.6	592.8	593.5	584	711.8
Co	16.8	28.9	14.0	12.8	6.6	17.4
Ni	310.2	389.7	382.3	377.3	336.5	381.1
Sc	21.0	18.0	18.1	18.1	18.2	19.6
V	143.1	153.7	125.1	132.5	122.7	144.7
Rb	327.1	495	635.9	662	701.9	434
Sr	1165.7	1045.3	684.2	671.5	564.8	1115
Ba	3660.7	3483.6	3887.8	3994.7	4056	3609.3
Nb	31.0	31.0	28.8	33.9	31.9	31.4
Ta	1.8	1.8	1.6	1.9	1.9	1.8
Zr	660.7	674.6	685	798.8	752.9	689.9
Hf	20.0	20.0	20.6	21.5	22.4	19.9
Y	17.4	20.6	17.5	14.8	12.8	17.1
Th	200.8	202.3	213.2	223.3	218.8	208.8
U	32.5	34.7	34.1	36.4	35.1	32.7
Pb	105.7	92.2	72.5	65.2	62.2	96.4
La	34.79	71.78	54.70	36.82	21.39	23.45
Ce	111.30	199.20	153.00	107.80	72.95	86.47
Pr	20.12	32.88	25.56	18.47	13.16	16.07
Nd	100.80	154.60	121.90	94.41	69.87	86.93
Sm	22.70	30.74	26.11	19.82	15.67	20.21
Eu	3.94	4.76	3.68	3.02	2.56	3.60
Gd	12.03	16.41	13.78	10.49	8.60	10.71
Tb	1.23	1.59	1.31	1.05	0.90	1.15
Dy	4.82	5.94	4.75	3.80	3.33	4.39
Ho	0.71	0.85	0.68	0.57	0.51	0.68
Er	1.80	2.25	1.71	1.38	1.22	1.62
Tm	0.21	0.24	0.19	0.16	0.15	0.20
Yb	1.36	1.59	1.24	1.11	1.04	1.31
Lu	0.20	0.23	0.18	0.18	0.16	0.19

Fe_2O_3T = Total Fe_2O_3 content; $Mg\# = 100 \times Mg^{2+}/(Mg^{2+} + Fe^{2+})$; $\delta Eu = Eu_N/(Sm_N \times Gd_N)^{1/2}$, subscript N presents chondrite normalization, the chondrite normalization values are from Sun and McDonough (1989).

* Data from Chen et al. (2012a).

REFERENCES

Ahmad T., Harris N., Bickle M., Chapman H., Bunbury J. and Prince C. (2000) Isotopic constraints on the structural relationships between the Lesser Himalayan Series and the High Himalayan Crystalline Series, Garhwal Himalaya. *Geol. Soc. Am. Bull.* **112**(3), 467–477.

Aikman A. B., Harrison T. M. and Hermann J. (2012) The origin of Eo- and Neo-himalayan granitoids, Eastern Tibet. *J. Asian Earth Sci.* **58**, 143–157.

Allegre C. J. and Turcotte D. L. (1986) Implications of a two-component marble-cake mantle. *Nature* **323**, 123–127.

Baker M. B., Hirschmann M. M., Ghiorso M. S. and Stolper E. M. (1995) Compositions of near-solidus peridotite melts from experiments and thermodynamic calculations. *Nature* **375**, 308–311.

Bas M. J. L., Maitre R. W. L., Streckeisen A. and Zanettin B. (1986) A chemical classification of volcanic rocks based on the total alkali-silica diagram. *J. Petrol.* **27**, 745–750.

Becker H., Carlson R. W. and Shirey S. B. (2004) Slab-derived osmium and isotopic disequilibrium in garnet pyroxenites from a Paleozoic convergent plate margin (lower Austria). *Chem. Geol.* **208**, 141–156.

Black L. R. and Jagodzinski E. A. (2003) Importance of establishing sources of uncertainty for the derivation of reliable SHRIMP ages. *Aust. J. Earth Sci.* **50**, 503–512.

Black L. P., Kamo S. L., Allen C. M., Aleinikoff J. N., Davis D. W., Korsch R. J. and Foudoulis C. (2003) TEMORA 1: a new zircon standard for Phanerozoic U–Pb geochronology. *Chem. Geol.* **200**, 155–170.

Blisniuk P. M., Hacker B. R., Glodny J., Ratschbacher L., Bi S. W., Wu Z. H., McWilliams M. O. and Calvert A. (2001) Normal faulting in central Tibet since at least 13.5 Myr ago. *Nature* **412**, 628–632.

Callegaro S., Marzoli A., Bertrand H., Chiaradia M., Reisberg L., Meyzen C., Bellieni G., Weems R. E. and Merle R. (2013) Upper and lower crust recycling in the source of CAMP basaltic dykes from southeastern North America. *Earth Planet. Sci. Lett.* **376**, 186–199.

Carlson R. W. and Nowell G. M. (2001) Olivine-poor sources for mantle-derived magmas: Os and Hf isotopic evidence from potassic magmas of the Colorado Plateau. *Geochem. Geophys. Geosyst.* **2**, paper number 2000GC000128.

Chen J. L. (2007) Geochemistry and origin of the Miocene potassic-ultrapotassic volcanic rocks in the Mid-Western Lhasa block, Tibetan plateau. Ph. D. thesis, Institute of Guangzhou Geochemistry, Chinese Academy of Sciences.

Chen J. L., Xu J. F., Wang B. D., Kang Z. Q. and Jie L. (2010) Origin of Cenozoic alkaline potassic volcanic rocks at KonglongXiang, Lhasa terrane, Tibetan Plateau: products of partial melting of a mafic lower-crustal source? *Chem. Geol.* **273**, 286–299.

Chen J. L., Xu J. F., Zhao W. X., Dong Y. H., Wang B. D. and Kang Z. Q. (2011) Geochemical variations in Miocene adakitic rocks from the western and eastern Lhasa terrane: implications for lower crustal flow beneath the southern Tibetan Plateau *Lithos* **125**, 928–939.

Chen J. L., Xu J. F., Wang B. D. and Kang Z. Q. (2012a) Cenozoic Mg-rich potassic rocks in the Tibetan Plateau: geochemical variations, heterogeneity of subcontinental lithospheric mantle and tectonic implications. *J. Asian Earth Sci.* **53**, 115–130.

Chen J. L., Zhao W. X., Xu J. F., Wang B. D. and Kang Z. Q. (2012b) Geochemistry of Miocene trachytes in Bugasi, Lhasa block, Tibetan Plateau: mixing products between mantle- and crust-derived melts? *Gondwana Res.* **21**, 112–122.

Chesley J., Ruiz J., Righter K., Ferrari L. and Gomez-Tuena A. (2002) Source contamination versus assimilation: an example from the Trans-Mexican Volcanic Arc. *Earth Planet. Sci. Lett.* **195**, 211–221.

Chu M. F., Chung S. L., Song B. A., Liu D. Y., O'Reilly S. Y., Pearson N. J., Ji J. Q. and Wen D. J. (2006) Zircon U–Pb and Hf isotope constraints on the Mesozoic tectonics and crustal evolution of southern Tibet. *Geology* **34**, 745–748.

Chung S. L., Liu D. Y., Ji J. Q., Chu M. F., Lee H. Y., Wen D. J., Lo C. H., Lee T. Y., Qian Q. and Zhang Q. (2003) Adakites from continental collision zones: melting of thickened lower crust beneath southern Tibet. *Geology* **31**, 1021–1024.

Chung S. L., Chu M. F., Zhang Y. Q., Xie Y. W., Lo C. H., Lee T. Y., Lan C. Y., Li X. H., Zhang Q. and Wang Y. Z. (2005) Tibetan tectonic evolution inferred from spatial and temporal variations in post-collisional magmatism. *Earth Sci. Rev.* **68**, 173–196.

Chung S. L., Chu M. F., Ji J. Q., O'Reilly S. Y., Pearson N. J., Liu D. Y., Lee T. Y. and Lo C. H. (2009) The nature and timing of crustal thickening in Southern Tibet: geochemical and zircon Hf isotopic constraints from postcollisional adakites. *Tectonophysics* **477**, 36–48.

Cohen A. S. and Waters F. G. (1996) Separation of osmium from geological materials by solvent extraction for analysis by thermal ionisation mass spectrometry. *Anal. Chim. Acta* **332**, 269–275.

Compston W., Williams I. S., Kirschvink J. L., Zichao Z. and Guogan M. A. (1992) Zircon U–Pb ages for the Early Cambrian Time-Scale. *J. Geol. Soc. London* **149**, 171–184.

Conticelli S., Carlson R. W., Widom E. and Serri G. (2007) Chemical and isotopic composition (Os, Pb, Nd, and Sr) of Neogene to Quaternary calc-alkalic, shoshonitic, and ultrapotassic mafi c rocks from the Italian peninsula: inferences on the nature of their mantle sources. In *Cenozoic Volcanism in the Mediterranean Area: Geol. Soc. Am. Spec. Paper* (eds. L. Beccaluva, G. Bianchini and M. Wilson), vol. 418. pp. 171–202. doi: 10.1130/2007.2418(09).

Creaser R. A., Papanastassiou D. A. and Wasserburg G. J. (1991) Negative thermal ion mass-spectrometry of osmium, rhenium, and iridium. *Geochim. Cosmochim. Acta* **55**, 397–401.

Day J. M. D., Pearson D. G., Macpherson C. G., Lowry D. and Carracedo J.-C. (2009) Pyroxenite-rich mantle formed by recycled oceanic lithosphere: oxygen-osmium isotope evidence from Canary Island lavas. *Geology* **37**, 555–558.

Ding L., Kapp P., Zhong D. L. and Deng W. M. (2003) Cenozoic volcanism in Tibet: evidence for a transition from oceanic to continental subduction. *J. Petrol.* **44**, 1833–1865.

Ding L., Yue Y., Cai F., Xu X., Zhang Q. and Lai Q. (2006) $^{40}Ar/^{39}Ar$ geochronology, geochemical and Sr–Nd–O isotopic characteristics of the high-Mg ultrapotassic rocks in Lhasa Block of Tibet: implications in the onset time and depth of NS-striking rift system. *Acta Geol. Sin.* **80**, 1252–1261.

Ellam R. M., Carlson R. W. and Shirey S. B. (1992) Evidence from Re–Os isotopes for plume-lithosphere mixing in Karoo flood basalt genesis. *Nature* **359**, 718–721.

Esser B. K. and Turekian K. K. (1993) The osmium isotopic composition of the continental crust. *Geochim. Cosmochim. Acta* **57**, 3093–3104.

Foley S. F., Venturelli G., Green D. H. and Toscani L. (1987) The ultrapotassic rocks – characteristics, classification, and constraints for petrogenetic models. *Earth Sci. Rev.* **24**, 81–134.

Foley S. (1992) Vein-plus-wall–rock melting mechanisms in the lithosphere and the origin of potassic alkaline magmas. *Lithos* **28**, 435–453.

Gannoun A., Burton K. W., Parkinson I. J., Alard O., Schiano P. and Thomas L. E. (2007) The scale and origin of the osmium

isotope variations in mid-ocean ridge basalts. *Earth Planet. Sci. Lett.* **259**, 541–556.

Gao Y. F., Hou Z. Q., Kamber B. S., Wei R. H., Meng X. J. and Zhao R. S. (2007a) Adakite-like porphyries from the southern Tibetan continental collision zones: evidence for slab melt metasomatism. *Contrib. Miner. Petrol.* **153**, 105–120.

Gao Y. F., Hou Z. Q., Kamber B. S., Wei R. H., Meng X. J. and Zhao R. S. (2007b) Lamproitic rocks from a continental collision zone: evidence for recycling of subducted Tethyan oceanic sediments in the mantle beneath southern Tibet. *J. Petrol.* **48**, 729–752.

Gao Y., Wei R., Ma P., Hou Z. and Yang Z. (2009) Post-collisional ultrapotassic volcanism in the Tangra Yumco-Xuruco graben, south Tibet: constraints from geochemistry and Sr–Nd–Pb isotope. *Lithos* **110**, 129–139.

Gao Y. F., Yang Z. S., Hou Z. Q., Wei R. H., Meng X. J. and Tian S. H. (2010) Eocene potassic and ultrapotassic volcanism in south Tibet: new constraints on mantle source characteristics and geodynamic processes. *Lithos* **117**, 20–32.

Guan Q., Zhu D. C., Zhao Z. D., Dong G. C., Zhang L. L., Li X. W., Liu M., Mo X. X., Liu Y. S. and Yuan H. L. (2012) Crustal thickening prior to 38Ma in southern Tibet: evidence from lower crust-derived adakitic magmatism in the Gangdese Batholith. *Gondwana Res.* **21**, 88–99.

Guo Z., Wilson M., Liu J. and Mao Q. (2006) Post-collisional, potassic and ultrapotassic magmatism of the northern Tibetan Plateau: constraints on characteristics of the mantle source, geodynamic setting and uplift mechanisms. *J. Petrol.* **47**, 1177–1220.

Guo Z., Wilson M., Zhang M., Cheng Z. and Zhang L. (2013) Post-collisional, K-rich mafic magmatism in south Tibet: constraints on Indian slab-to-wedge transport processes and plateau uplift. *Contrib. Miner. Petrol.* **165**, 1311–1340.

Guo Z. F., Wilson M. and Liu J. Q. (2007) Post-collisional adakites in south Tibet: products of partial melting of subduction-modified lower crust. *Lithos* **96**, 205–224.

Gurenko A. A., Sobolev A. V., Hoernle K. A., Hauff F. and Schmincke H.-U. (2009) Enriched, HIMU-type peridotite and depleted recycled pyroxenite in the Canary plume: a mixed-up mantle. *Earth Planet. Sci. Lett.* **277**, 514–524.

Hart S. R. and Ravizza G. E. (1996) Os partitioning between phases in lherzolite and basalt. In *Earth Processes: Reading the Isotopic Code*, vol. 95, pp. 123–134. Earth Processes: Reading the Isotopic Code. AGU, Washington, DC.

Hart W. K., Carlson R. W. and Shirey S. B. (1997) Radiogenic Os in primitive basalts from the northwestern U.S.A.: implications for petrogenesis. *Earth Planet. Sci. Lett.* **150**, 103–116.

Harvey J., Gannoun A., Burton K. W., Schiano P., Rogers N. W. and Alard O. (2010) Unravelling the effects of melt depletion and secondary infiltration on mantle Re–Os isotopes beneath the French Massif Central. *Geochim. Cosmochim. Acta* **74**, 293–320.

Harvey J., Dale C. W., Gannoun A. and Burton K. W. (2011) Osmium mass balance in peridotite and the effects of mantle-derived sulphides on basalt petrogenesis. *Geochim. Cosmochim. Acta* **75**, 5574–5596.

Hattori Y., Suzuki K., Honda M. and Shimizu H. (2003) Re–Os isotope systematics of the Taklimakan Desert sands, moraines and river sediments around the Taklimakan Desert, and of Tibetan soils. *Geochim. Cosmochim. Acta* **67**, 1195–1205.

Herzberg C. (2011) Identification of source lithology in the Hawaiian and Canary islands: implications for origins. *J. Petrol.* **52**, 113–146.

Herzberg C. and Asimow P. D. (2008) Petrology of some oceanic island basalts: PRIMELT2.XLS software for primary magma calculation. *Geochem. Geophys. Geosyst.* **9**. http://dx.doi.org/10.1029/2008GC002057.

Hirschmann M. M. and Stolper E. M. (1996) A possible role for garnet pyroxenite in the origin of the "garnet signature" in MORB. *Contrib. Miner. Petrol.* **124**, 185–208.

Hirschmann M. M., Kogiso T., Baker M. B. and Stolper E. M. (2003) Alkalic magmas generated by partial melting of garnet pyroxenite. *Geology* **31**, 481–484.

Hoskin P. W. O. and Schaltegger U. (2003) The composition of zircon and igneous and metamorphic petrogenesis. *Rev. Mineral. Geochem.* **53**, 27–62.

Hou Z. Q., Gao Y. F., Qu X. M., Rui Z. Y. and Mo X. X. (2004) Origin of adakitic intrusives generated during mid-Miocene east-west extension in southern Tibet. *Earth Planet. Sci. Lett.* **220**, 139–155.

Ji W. Q., Wu F. Y., Chung S. L., Li J. X. and Liu C. Z. (2009) Zircon U–Pb geochronology and Hf isotopic constraints on petrogenesis of the Gangdese batholith, southern Tibet. *Chem. Geol.* **262**, 229–245.

Jian P., Kroner A. and Zhou G. Z. (2012) SHRIMP zircon U–Pb ages and REE partition for high-grade metamorphic rocks in the North Dabie complex: insight into crustal evolution with respect to Triassic UHP metamorphism in east-central China. *Chem. Geol.* **328**, 49–69.

Kapp P., DeCelles P. G., Gehrels G. E., Heizier M. and Ding L. (2007) Geological records of the Lhasa-Qiangtang and Indo-Asian collisions in the Nima area of central Tibet. *Geol. Soc. Am. Bull.* **119**, 917–932.

Kohn M. J. and Parkinson C. D. (2002) Petrologic case for Eocene slab breakoff during the Indo-Asian collision. *Geology* **30**, 591–594.

Langmuir C. H., Vocke R. D., Hanson G. N. and Hart S. R. (1978) General mixing equation with applications to icelandic basalts. *Earth Planet. Sci. Lett.* **37**, 380–392.

Lee H. Y., Chung S. L., Lo C. H., Ji J. Q., Lee T. Y., Qian Q. and Zhang Q. (2009) Eocene Neotethyan slab breakoff in southern Tibet inferred from the Linzizong volcanic record. *Tectonophysics* **477**, 20–35.

Lee H. Y., Chung S. L., Ji J., Qian Q., Gallet S., Lo C. H., Lee T. Y. and Zhang Q. (2012) Geochemical and Sr–Nd isotopic constraints on the genesis of the Cenozoic Linzizong volcanic successions, southern Tibet. *J. Asian Earth Sci.* **53**, 96–114.

Li X. H., Liu D. Y., Sun M., Li W. X., Liang X. R. and Liu Y. (2004) Precise Sm–Nd and U–Pb isotopic dating of the super-giant Shizhuyuan polymetallic deposit and its host granite, Southeast China. *Geol. Magz.* **141**, 225–231.

Li J., Xu J. F., Suzuki K., He B., Xu Y. G. and Ren Z. Y. (2010) Os, Nd and Sr isotope and trace element geochemistry of the Muli picrites: insights into the mantle source of the Emeishan Large Igneous Province. *Lithos* **119**, 108–122.

Li J., Jiang X. Y., Xu J. F., Zhong L. F., Wang X. C., Wang G. Q. and Zhao P. P. (2014) Determination of platinum-group elements and Re-Os isotopes using ID-ICP-MS and N-TIMS from a single digestion after two-dtage column separation. *Geostand. Geoanal. Res.* **38**, 37–50.

Liao S., Chen Z., Luo Z. and Zhou A. (2002) Discovery of leucite phonolite in the Tangra Yumco area, Tibet and its geological significance. *Geol. Bull. China* **21**, 735–738.

Liao Z. L., Mo X. X., Pan G. T., Zhu D. C., Wang L. Q., Jiang X. S. and Zhao Z. D. (2007) Spatial and temporal distribution of peraluminous granites in Tibet and their tectonic significance. *J. Asian Earth Sci.* **29**(2–3), 378–389.

Liu Y., Gao S., Lee C. T., Hu S., Liu X. and Yuan H. (2005) Melt-peridotite interactions: links between garnet pyroxenite and high-Mg# signature of continental crust. *Earth Planet. Sci. Lett.* **234**, 39–57.

Liu Y. S., Gao S., Kelemen P. B. and Xu W. L. (2008) Recycled crust controls contrasting source compositions of Mesozoic and

Cenozoic basalts in the North China Craton. *Geochim. Cosmochim. Acta* **72**, 2349–2376.

Liu C. Z., Wu F. Y., Chung S. L. and Zhao Z. D. (2011) Fragments of hot and metasomatized mantle lithosphere in Middle Miocene ultrapotassic lavas, southern Tibet. *Geology* **39**, 923–926.

Liu D., Zhao Z., Zhu D. C., Niu Y. and Harrison T. M. (2013) Zircon xenocrysts in Tibetan ultrapotassic magmas: imaging the deep crust through time. *Geology*. http://dx.doi.org/10.1130/G34902.1.

Liu C. Z., Wu F. Y., Chung S. L., Li Q. L., Sun W. D. and Ji W. Q. (2014a) A 'hidden' ^{18}O-enriched reservoir in the sub-arc mantle. *Sci. Rep.*. http://dx.doi.org/10.1038/srep04232.

Liu D., Zhao Z., Zhu D. C., Niu Y., DePaolo D. J., Harrison T. M., Mo X., Dong G., Zhou S., Sun C., Zhang Z. and Liu J. (2014b) Postcollisional potassic and ultrapotassic rocks in southern Tibet: mantle and crustal origins in response to India-Asia collision and convergence. *Geochim. Cosmochim. Acta*, http://dx.doi.org/10.1016/j.gca.2014.03.031.

Maheo G., Guillot S., Blichert-Toft J., Rolland Y. and Pecher A. (2002) A slab breakoff model for the Neogene thermal evolution of South Karakorum and South Tibet. *Earth Planet. Sci. Lett.* **195**, 45–58.

Meisel T., Walker R. J. and Morgan J. W. (1996) The osmium isotopic composition of the Earth's primitive upper mantle. *Nature* **383**, 517–520.

Meisel T., Walker R. J., Irving A. J. and Lorand J.-P. (2001) Osmium isotopic compositions of mantle xenoliths: a global perspective. *Geochim. Cosmochim. Acta* **65**, 1311–1323.

Miller C., Schuster R., Klötzli U., Frank W. and Purtscheller F. (1999) Post-collisional potassic and ultrapotassic magmatism in SW Tibet: geochemical and Sr–Nd–Pb–O isotopic constraints for mantle source characteristics and petrogenesis. *J. Petrol.* **40**, 1399–1424.

Mo X., Hou Z., Niu Y., Dong G., Qu X., Zhao Z. and Yang Z. (2007) Mantle contributions to crustal thickening during continental collision: evidence from Cenozoic igneous rocks in southern Tibet. *Lithos* **96**, 225–242.

Mo X. X., Niu Y. L., Dong G. C., Zhao Z. D., Hou Z. Q., Zhou S. and Ke S. (2008) Contribution of syncollisional felsic magmatism to continental crust growth: a case study of the Paleogene Linzizong volcanic Succession in southern Tibet. *Chem. Geol.* **250**, 49–67.

Nier A. O. (1950) A redetermination of the relative abundances of the isotopes of carbon, nitrogen, oxygen, argon, and potassium. *Phys. Rev.* **77**, 789–793.

Owens T. J. and Zandt G. (1997) Implications of crustal property variations for models of Tibetan plateau evolution. *Nature* **387**, 37–43.

Pan G., Wang L., Li R., Yuan S., Ji W., Yin F., Zhang W. and Wang B. (2012) Tectonic evolution of the Qinghai-Tibet Plateau. *J. Asian Earth Sci.* **53**, 3–14.

Pearson D. G. and Woodland S. J. (2000) Solvent extraction/anion exchange separation and determination of PGEs (Os, Ir, Pt, Pd, Ru) and Re–Os isotopes in geological samples by isotope dilution ICP-MS. *Chem. Geol.* **165**, 87–107.

Pertermann M. and Hirschmann M. M. (2003) Anhydrous partial melting experiments on MORB-like eclogite: phase relations, phase compositions and mineral-melt partitioning of major elements at 2–3 GPa. *J. Petrol.* **44**, 2173–2201.

Prelevic D., Akal C., Foley S. F., Romer R. L., Stracke A. and Van Den Bogaard P. (2012) Ultrapotassic mafic rocks as geochemical proxies for post-collisional dynamics of orogenic lithospheric mantle: the case of southwestern Anatolia. *Turkey. J. Petrol.* **53**, 1019–1055.

Richards A., Argles T., Harris N., Parrish R., Ahmad T., Darbyshire F. and Draganits E. (2005) Himalayan architecture constrained by isotopic tracers from clastic sediments. *Earth Planet. Sci. Lett.* **236**, 773–796.

Rowley D. B. (1996) Age of initiation of collision between India and Asia: a review of stratigraphic data. *Earth Planet. Sci. Lett.* **145**, 1–13.

Royden L. H., Burchfiel B. C. and van der Hilst R. D. (2008) The geological evolution of the Tibetan plateau. *Science* **321**, 1054–1058.

Schaefer B. F., Turner S. P., Rogers N. W., Hawkesworth C. J., Williams H. M., Pearson D. G. and Nowell G. M. (2000) Re–Os isotope characteristics of postorogenic lavas: implications for the nature of young lithospheric mantle and its contribution to basaltic magmas. *Geology* **28**, 563–566.

Shirey S. B. and Walker R. J. (1995) Carius tube digestion for low-blank rhenium–osmium analysis. *Anal. Chem.* **67**, 2136–2141.

Shirey S. B. and Walker R. J. (1998) The Re–Os isotope system in cosmochemistry and high-temperature geochemistry. *Annu. Rev. of Earth Planet. Sci.* **26**, 423–500.

Sobolev A. V., Hofmann A. W., Sobolev S. V. and Nikogosian I. K. (2005) An olivine-free mantle source of Hawaiian shield basalts. *Nature* **434**, 590–597.

Sobolev A. V., Hofmann A. W., Kuzmin D. V., Yaxley G. M., Arndt N. T., Chung S. L., Danyushevsky L. V., Elliott T., Frey F. A., Garcia M. O., Gurenko A. A., Kamenetsky V. S., Kerr A. C., Krivolutskaya N. A., Matvienkov V. V., Nikogosian I. K., Rocholl A., Sigurdsson I. A., Sushchevskaya N. M. and Teklay M. (2007) The amount of recycled crust in sources of mantle-derived melts. *Science* **316**, 412–417.

Sobolev A. V., Hofmann A. W., Brügmann G., Batanova V. G. and Kuzmin D. V. (2008) A quantitative link between recycling and osmium isotopes. *Science* **321**, 536.

Sun S. S. and McDonough W. F. (1989) Chemical and isotopic systematics of oceanic basalts: implications for mantle composition and processes. *Geol. Soc. London Spec. Publ.* **42**, 313–345.

Turner S., Arnaud N., LIU J., Rogers N., Hawkesworth C., Harris N., Kelley S., Van Calsteren P. and Deng W. (1996) Post-collision, shoshonitic volcanism on the Tibetan Plateau: implications for convective thinning of the lithosphere and the source of ocean island basalts. *J. Petrol.* **37**, 45–71.

Volkening J., Walczyk T. and Heumann K. G. (1991) Osmium isotope ratio determinations by negative thermal ionization mass-spectrometry. *Int. J. Mass Spectrom.* **105**, 147–159.

Walker R. J., Carlson R. W., Shirey S. B. and Boyd F. R. (1989) Os, Sr, Nd, and Pb isotope systematics of southern African peridotite xenoliths: implications for the chemical evolution of subcontinental mantle. *Geochim. Cosmochim. Acta* **53**, 1583–1595.

Walker R. J., Prichard H. M., Ishiwatari A. and Pimentel M. (2002) The osmium isotopic composition of convecting upper mantle deduced from ophiolite chromites. *Geochim. Cosmochim. Acta* **66**, 329–345.

Wang B., Chen J., Xu J. and Wang L. (2014) Geochemical and Sr–Nd–Pb–Os isotopic compositions of Miocene ultrapotassic rocks in southern Tibet: petrogenesis and implications for the regional tectonic history. *Lithos* **208–209**, 237–250.

Wang B., Xu J., Zhang X., Chen J., Kang Z. and Dong Y. (2008) Petrogenesis of Miocene volcanic rocks in the Sailipu area, Western Tibetan Plateau: geochemical and Sr–Nd isotopic constraints. *Acta Petrol Sin* **24**, 265–278.

Wei G. J., Liang X. R., Li X. H. and Liu Y. (2002) Precise measurement of Sr isotopic composition of liquid and solid base using (LP) MC-ICPMS. *Geochimica* **31**, 295–299.

Widom E. and Shirey S. B. (1996) Os isotope systematics in the Azores: implications for mantle plume sources. *Earth Planet. Sci. Lett.* **142**, 451–465.

Williams I. S., Buick I. S. and Cartwright I. (1996) An extended episode of early Mesoproterozoic metamorphic fluid flow in the Reynolds Range, central Australia. *J. Metamorph. Geol.* **14**, 29–47.

Williams H. M., Turner S. P., Pearce J. A., Kelley S. P. and Harris N. B. W. (2004) Nature of the source regions for post-collisional, potassic magmatism in southern and northern Tibet from geochemical variations and inverse trace element modelling. *J. Petrol.* **45**, 555–607.

Xie G., Zou A., Yuan J., Li X., Liao S., Tang F., Huang C., Chen Z. and Xu Z. (2004) New results and major progress in regional geological survey of the Boindoi district and Comai sheets. *Geol. Bull. China* **23**, 498–505.

Xu J. F., Suzuki K., Xu Y. G., Mei H. J. and Li J. (2007) Os, Pb, and Nd isotope geochemistry of the Permian Emeishan continental flood basalts: Insights into the source of a large igneous province. *Geochim. Cosmochim. Acta* **71**, 2104–2119.

Yaxley G. M. and Green D. H. (1998) Reactions between eclogite and peridotite: mantle refertilisation by subduction of oceanic crust. *Mineral. Petrogr. Mitt.* **78**, 243–255.

Yin A. and Harrison T. M. (2000) Geologic evolution of the Himalayan–Tibetan orogen. *Annu. Rev. Earth Plant. Sci.* **28**, 211–280.

Zhang Z., Dong X., Xiang H., Liou J. G. and Santosh M. (2013) Building of the deep Gangdese Arc, South Tibet: Paleocene plutonism and granulite-facies metamorphism. *J. Petrol.* **54**, 2547–2580.

Zhao Z., Mo X., Nomade S., Renne P. R., Zhou S., Dong G., Wang, Zhu D. and Liao Z. (2006) Post-collisional ultrapotassic rocks in Lhasa Block, Tibetan Plateau: spatial and temporal distribution and it's implications. *Acta Petrol. Sin.* **22**, 787–794.

Zhao Z., Mo X., Sun C., Zhu D., Niu Y., Dong G., Zhou S., Dong X. and Liu Y. (2008) Mantle xenoliths in southern Tibet: geochemistry and constraints for the nature of mantle. *Acta Petrol. Sin.* **24**, 193–202.

Zhao Z. D., Mo X. X., Dilek Y., Niu Y. L., DePaolo D. J., Robinson P., Zhu D. C., Sun C. G., Dong G. C., Zhou S., Luo Z. H. and Hou Z. Q. (2009) Geochemical and Sr–Nd–Pb–O isotopic compositions of the post-collisional ultrapotassic magmatism in SW Tibet: petrogenesis and implications for India intra-continental subduction beneath southern Tibet. *Lithos* **113**, 190–212.

Zhou S., Xuanxue M., Guochen D., Zhidan Z., Ruizhao Q., Tieying G. and Liangliang W. (2004) 40Ar-39Ar geochronology of Cenozoic Linzizong volcanic rocks from Linzhou Basin, Tibet, China, and their geological implications. *Chinese Sci. Bull.* **49**, 1970–1979.

Zhou S., Mo X. X., Zhao Z. D. and Qiu R. Z. (2009) Spatial and temporal distribution and petrogenesis of Miocene ultrapotassic volcanism in Gangdese, Tibet. *Geochim. Cosmochim. Acta* **73**. A1527-A1527.

Zhu D. C., Zhao Z. D., Niu Y. L., Mo X. X., Chung S. L., Hou Z. Q., Wang L. Q. and Wu F. Y. (2011) The Lhasa Terrane: record of a microcontinent and its histories of drift and growth. *Earth Planet. Sci. Lett.* **301**, 241–255.

Zhu D. C., Zhao Z. D., Niu Y., Dilek Y., Hou Z. Q. and Mo X. X. (2013) The origin and pre-Cenozoic evolution of the Tibetan Plateau. *Gondwana Res.* **23**, 1429–1454.

Associate editor: Weidong Sun